Report no. changed (Mar 2006): SM-368-UU

SACLANTCEN MEMORANDUM
serial no: SM- 368

SACLANT UNDERSEA RESEARCH CENTRE REPORT

Application of aided inertial navigation system to synthetic aperture sonar micronavigation

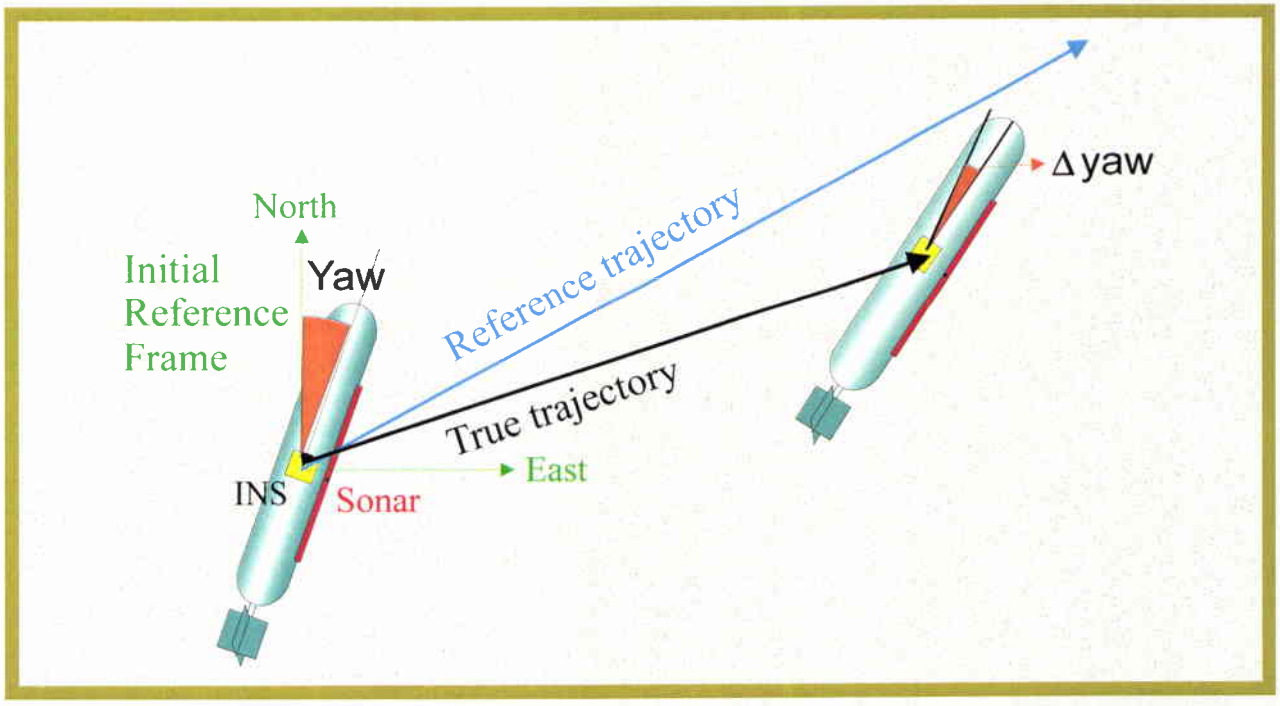

Alessandra Tesei, Marc Pinto

January 2001

NORTH ATLANTIC TREATY ORGANIZATION ORGANISATION DU TRAITE DE L'ATLANTIQUE NORD

Application of Aided Inertial Navigation System to Synthetic Aperture Sonar Micronavigation

A. Tesei and M. Pinto

The content of this document pertains to work performed under Project 03-G of the SACLANTCEN Programme of Work. The document has been approved for release by The Director, SACLANTCEN.

Jan L. Spoelstra
Director

intentionally blank page

Application of Aided Inertial Navigation System to Synthetic Aperture Sonar Micronavigation

A. Tesei and M. Pinto

Executive Summary: Image quality is considered a major issue in order to classify a detected MIne-Like ECho (MILEC) as a MIne-Like COntact (MILCO). Synthetic Aperture Sonar (SAS) is proposed for increasing the sonar cross-range resolution, hence to provide high-resolution images. Short-term, high precision navigation has been recognized as critical to SAS image quality. Short-term navigation is the positioning and attitude estimation of the underwater vehicle travelling over the time interval of a typical SAS aperture (i.e., 100 s maximum).

To the purpose of promoting research in this field SACLANTCEN has recently procured a high precision Aided INS (AINS) consisting of inertial navigation system (INS), Doppler Velocity Log (DVL), depth meter and intermittent DGPS fixes. This report describes and predicts by theoretical investigation and simulation the short-term navigational accuracy of the INS system operating in free-inertial mode.

By modelling the main components of INS measurement errors and performing error analysis, the feasibility of short-term free inertial navigation is evaluated with respect to the accuracy constraints imposed by SAS processing. By means of *N*avlab, a navigational simulator/estimator provided by NDRE (Norwegian Defence Research Establishment), this theoretical error analysis is statistically validated on a simulated typical mission configuration. Although the selected strapdown INS is one of the best available, providing very accurate attitude measurements, its accuracy in positioning is insufficient when compared with SAS requirements.

Future research will address the reduction of low-frequency residual position errors by designing an architecture to integrate the INS measurement with traditional aiding navigation sensors (DGPS, Doppler Velocity Log, depth meter, etc.), as in standard Aided Inertial Navigation Systems (AINS), and SAS-based micronavigation techniques.

After preliminary tests, this navigation system will be installed on an Autonomous Underwater Vehicle (AUV) for AUV navigation and SAS processing to determine whether image quality gives the classification capability.

intentionally blank page

Application of Aided Inertial Navigation System to Synthetic Aperture Sonar Micronavigation

A. Tesei and M. Pinto

Abstract: In order to improve short-term navigational accuracy, critical to successful SAS processing, a high-quality Inertial Navigation System (INS) is investigated, which consists of an inertial measurement unit (IMU) and a strapdown navigator. Although the strapdown INS recently acquired at SACLANTCEN is one of the best available, the accuracy of positioning remains insufficient, in particular for high-frequency SAS. The INS performance was predicted via ψ-angle error analysis of the navigation equations and a navigational simulator/estimator provided by NDRE (Norwegian Defence Research Establishment). The short-term residual errors of position and attitude displacement were analyzed in terms of dominant measurement error components and their sources. Preliminary results show that the attitude error is negligible due to the low values of gyro bias and white noise. The position displacement error is dominated by a quadratic drift due to accelerometer bias. Integrating the INS with additional navigation sensors (e.g., Doppler Velocity Log, depth meter, etc.) and SAS motion compensation techniques by means of an appropriate fusion architecture will significantly reduce the most critical error components. The design, development and test of the combined SAS-INS architecture will be the main objective of future work.

Keywords: Inertial Navigation Systems ∘ Short-term error mechanisms ∘ Micronavigation

Contents

1

Introduction

Short-term, high precision navigation is critical to Synthetic Aperture Sonar (SAS) processing. Short-term navigation is defined as the positioning and attitude estimation of an underwater vehicle travelling over the time interval corresponding to a typical SAS aperture (namely, SAS Integration Time - SASIT). The maximum extension of this time interval is of the order of 100 s.

The sensor package incorporated in a recently procured very high precision Aided Inertial Navigation System (AINS) consists of an inertial navigation system (INS), Doppler velocity log, depth meter and intermittent DGPS fixes. The data acquired are fused by an extended Kalman filter. After preliminary tests, this navigation system will be installed on an Autonomous Underwater Vehicle (AUV) where it will be used for AUV navigation and SAS processing.

This report describes and predicts by theoretical investigation and simulation the short-term navigational accuracy of the INS system which is included in the AINS package, and assumes to work in free-inertial mode. Through the modelling of main components of inertial sensor measurement errors and ψ-angle error analysis of the strapdown navigation equation mechanism, the feasibility of short-term, free inertial navigation is evaluated under the accuracy constraints imposed by SAS processing and its most critical limitations are outlined.

Error analysis is performed at short term (over a typical SAS aperture) and separately on the error components introduced by the inertial measurement unit (Sect. 2). The maximum error budget accepted on vehicle positioning and attitude computation is established according to the navigational precision requirements of position and attitude displacement errors imposed by SAS processing along an aperture (Sect. 3). The theoretical analysis is statistically validated on a simulated typical mission configuration using NavLab, a navigational simulator/estimator provided by NDRE (Norwegian Defence Research Establishment) (Sect. 3).

A subsequent report will describe the integration of the INS with the additional sensors included in the AINS. Accuracy will be evaluated from a theoretical point of view and by simulation.

Although the selected strapdown INS is one of the best available, the accuracy

of positioning is expected to remain insufficient, in particular for high-frequency Synthetic Aperture Sonar (SAS) [1]. Aiding the AINS-based navigation with SAS motion compensation techniques by means of an appropriate fusion architecture will significantly reduce some of the residual error contributions, in particular those low-frequency residual error contributions related to constant accelerometer bias which causes significantly high quadratic position displacement errors. Future research will address fusion architecture design to improve short-term navigation accuracy by merging the SAS-based micronavigation approach [2][3] with the more traditional AINS-based methodology.

2

An Inertial Navigation System (INS) for micronavigation

The use of a traditional INS system for short-term high precision navigation is described. Positioning accuracy is evaluated by theoretical investigation. The results of this study are confirmed by simulation in Section 3.

The basic component of a typical AINS system, i.e., the strapdown Inertial Navigation System (INS), is described, and its error modelling and mechanization are proposed.

2.1 Mathematical notation

In order to describe the navigation system and error mechanization a suitable notation was defined (Table 1) [4].

The specific dynamic vectors involved in the navigation system are defined in Table 2 [4]. Whenever the symbol superscript C shown in the table is omitted, the related reference frame is assumed to coincide with the frame A of the symbol subscript.

2.2 The strapdown Inertial Navigation System

The strapdown INS consists of an Inertial Measurement Unit (IMU), its platform and an inertial navigation system. The IMU sensors are three accelerometers and a 3-axis gyro. On the basis of the inertial measurements provided by the IMU, a suitable navigator is designed which is devoted to describe the sensor platform and the vehicle dynamics with respect to the Earth.

Inertial navigation systems solve the Newton's force equations from measurements (i.e, the accelerometer outputs) of specific force applied to the body and coordinatized in a frame the orientation of which with respect to an inertial frame is known via the three-axes gyro. For "body" (b) the sensor platform is intended. This must

Symbol	Description
$\vec{k}$	coordinate free (or "symbolic") generic vector (not decomposed in any coordinate system)
K	matrix
$\frac{d}{dt}\vec{k}\Big\|^C$	time derivation computed in the coordinate system C
$\mathbf{k}_{AB}^C$	generic vector defining the linear position, velocity or acceleration of the origin of the coordinate system B relative to the coordinate system A (as well as attitude, angular rate or acceleration of the B frame with respect to the A frame), decomposed in the reference frame C

Table 1 *General mathematical notation.*

be installed on the vehicle so that its axes (Roll, Pitch and Yaw) are aligned with the vehicle Bow, Starboard and Down respectively (Annex A).

If a generic rotating frame, r, is used as reference frame with respect to which to compute time derivations, the change with time of the body linear speed, $\vec{v}_{eb}$, with respect to the ground (i.e., to the Earth e) is expressed in terms of the body speed referred to the Inertial system (i), $\vec{v}_{ib}$, as follows:

$$\frac{d}{dt}\vec{v}_{eb}\Big|^r = \frac{d}{dt}\vec{v}_{ib}\Big|^r - \vec{\omega}_{ie} \wedge (\vec{\omega}_{ie} \wedge \vec{p}_{eb}) - (2\vec{\omega}_{ie} + \vec{\omega}_{er}) \wedge \vec{v}_{eb}. \tag{1}$$

The vector $\vec{p}_{eb}$ is the body position with respect to the Earth. The term $\vec{\omega}_{ie} \wedge (\vec{\omega}_{ie} \wedge \vec{p}_{eb})$ represents the centripetal acceleration, the term $2\vec{\omega}_{ie} \wedge \vec{v}_{eb}$ the Coriolis effect; the term $\vec{\omega}_{er} \wedge \vec{v}_{eb}$ is due to the rotation of the reference frame r. The relation between the body position derivative computed in the r frame and the same derivative computed in the Earth-fixed (e) frame is:

$$\frac{d}{dt}\vec{p}_{eb}\Big|^e = \frac{d}{dt}\vec{p}_{eb}\Big|^r + \vec{\omega}_{er} \wedge \vec{p}_{eb}. \tag{2}$$

The reference frames further than r, that is b, e and i, are the Body, the Earth-fixed and the Inertial frames are defined in Annex A. Notice that the term $\frac{d}{dt}\vec{v}_{ib}\Big|^r$ corresponds to the acceleration ${}^r\vec{a}_{ib}$ that can be expressed as the sum of the inertial specific force $\vec{f}_{ib}$ sensed by the body and the Earth mass attraction $\vec{g}_{ib}$:

$$\frac{d}{dt}\vec{v}_{ib}\Big|^r = {}^r\vec{a}_{ib} = \vec{f}_{ib} + \vec{g}_{ib}. \tag{3}$$

Hence Eq. (1) can be rewritten as:

$$\frac{d}{dt}\vec{v}_{eb}\Big|^r = \vec{f}_{ib} + \vec{g}_{ib} - \vec{\omega}_{ie} \wedge (\vec{\omega}_{ie} \wedge \vec{p}_{eb}) - (2\vec{\omega}_{ie} + \vec{\omega}_{er}) \wedge \vec{v}_{eb}. \tag{4}$$

Symbol	Definition	Description
$\vec{p}_{AB}$		Position vector of the origin of the coordinate system B relative to the coordinate system A (i.e., the vector starts from A origin and points to the B origin)
${}^{C}\vec{v}_{AB}$	$\frac{d}{dt}\vec{p}_{AB}\Big\vert^{C} = {}^{C}\dot{\vec{p}}_{AB}$	linear velocity of the B origin relative to the A origin, observed from the C frame
${}^{C}\vec{a}_{AB}$	$\frac{d}{dt}\vec{v}_{AB}\Big\vert^{C} = {}^{C}\dot{\vec{v}}_{AB}$	linear acceleration of the B system origin relative to the A system origin, observed from the C frame
$\vec{\omega}_{AB}$		angular velocity (or rate) of the coordinate system B relative to the coordinate system A

Table 2 *Definition and notation of the main dynamic quantities.*

We can define the gravity vector $\vec{g'}_{ib}$ as the combination of the Earth mass attraction, $\vec{g}_{ib}$, and the centripetal acceleration due to the Earth rotation. It is a vector pointing towards the Earth geodetic centre, i.e., follows the perpendicular to the Earth surface at the current location:

$$\vec{g'}_{ib} = \vec{g}_{ib} - \vec{\omega}_{ie} \wedge (\vec{\omega}_{ie} \wedge \vec{p}_{eb}). \tag{5}$$

Now Eq. (4) can be rearranged as follows:

$$\frac{d}{dt}\vec{v}_{eb}\Big\vert^{r} = \vec{f}_{ib} + \vec{g'}_{ib} - (2\vec{\omega}_{ie} + \vec{\omega}_{er}) \wedge \vec{v}_{eb}. \tag{6}$$

If all the involved dynamic quantities are now coordinatized in the generic r frame, Eq. (6) becomes:

$$\dot{\mathbf{v}}^{r}_{eb} = \mathbf{f}^{r}_{ib} + \mathbf{g'}^{r}_{ib} - (2\omega^{r}_{ie} + \omega^{r}_{er}) \wedge \mathbf{v}^{r}_{eb}. \tag{7}$$

In order to **navigate over large distances** (order of some km), navigation information is commonly computed in the current *local* geographic reference frame l (also called *navigation* or "North, East, Down" (NED) frame), described in terms of north and east components, longitude, latitude and height and referred to the Earth. This is called local frame mechanization and the related navigation equation is obtained by substituting r with l in Eq. (7). It simplifies the representation of the Earth's gravitational field and is suitable for taking into account the curvature of the Earth.

In this mechanization the force $\mathbf{f}^{l}_{ib}$ can be expressed in terms of the same force as sensed by the IMU, i.e., coordinatized in the body frame:

$$\mathbf{f}^{l}_{ib} = C^{l}_{b}\mathbf{f}^{b}_{ib}, \tag{8}$$

where C_b^l is the Direction Cosine Matrix (DCM) used to transform a vector measured by the IMU (hence related to the body frame) into the local axes (see Annex A). This matrix propagates according to the equation:

$$\dot{C}_b^l = C_b^l \Omega_{lb}^b, \tag{9}$$

where Ω_{lb}^b is the skew symmetric form of ω_{lb}^b, i.e., the body rate with respect to the navigation frame, decomposed in the body frame. This quantity can be derived from the body angular rate with respect to the inertial frame (measured by the IMU), ω_{ib}^b, and the computed angular rate of the navigation local frame with respect to the inertial axes, ω_{il}^b. The latter term comes from the sum of the Earth's angular rate re the inertial frame (ω_{ie}^l) and the transport rate of the local frame (ω_{el}^l). Hence:

$$\omega_{lb}^b = \omega_{ib}^b - \omega_{il}^b = \omega_{ib}^b - C_l^b(\omega_{ie}^l + \omega_{el}^l). \tag{10}$$

The Earth rotation rate relative to the inertial frame, which is represented by a vector with constant modulus Ω directed along the polar axis pointing to the North, is represented in the l frame as:

$$\omega_{ie}^l = C_e^l \omega_{ie}^e = [\Omega \cos(lat), \quad 0, \quad -\Omega \sin(lat)]^T. \tag{11}$$

If the body velocity with respect to the Earth represented in the l frame is defined as $\mathbf{v}_{eb}^l = [v_N, \quad v_E, \quad v_D]^T$, then it is easy to express ω_{el}^l in terms of geographical coordinates (in particular, latitude, lat, and altitude, h) and $\mathbf{v}_{eb}^l$:

$$\omega_{el}^l = [\frac{v_E}{R_E + h}, \quad \frac{-v_N}{R_N + h}, \quad \frac{-v_E \tan(lat)}{R_N + h}]^T. \tag{12}$$

Notice that h is conventionally positive above the sea level. Equation (12) is valid when the Earth model is ellipsoidal, in which case the following definitions are applied:

$$\begin{aligned} R_E &= \frac{\bar{R}}{(1-e^2 \sin^2(lat))^{1/2}} \\ R_N &= \frac{\bar{R}(1-e^2)}{(1-e^2 \sin^2(lat))^{3/2}} \\ \bar{R} &= \sqrt{R_E R_N} \end{aligned} \tag{13}$$

where the quantities $\bar{R}$ and e are defined according to Table 3 and set up by selecting the geodetic WGS-84 model as reference ellipsoid. As in first approximation we assume the Earth to be spherical, then $R_E = R_N = \bar{R}$.

Finally, the position vector $\mathbf{p}_{eb}^l$ has as magnitude the sum of the altitude h (assumed positive above the sea level) and the distance R_{el} between the Local frame origin and the Earth centre, and, under the hypothesis of spherical Earth, is directed along the Down axis:

$$\mathbf{p}_{eb}^l = [0, \quad 0, \quad -(R_{el} + h)]^T; \tag{14}$$

hence the gravity vector as seen from the l frame can be expressed as:

$$\mathbf{g}'^l_{ib} = \mathbf{g}_{ib}^l - \frac{\Omega^2(R_{el} + h)}{2} [\sin(2lat), \quad 0, \quad (1 + \cos(2lat)]^T. \tag{15}$$

Ellipsoid parameter	Symbol	Value (WGS84)
Equatorial radius	$\bar{R}$	6378137.0 m
Polar radius	$\bar{r}$	6356752.3142 m
flattening	$f = (\bar{R} - \bar{r})/\bar{R}$	1/298.257223563
major eccentricity	$e = \sqrt{f(2-f)}$	0.0818191908426
Earth rate	Ω	$7.292115(10^{-5})$ rad/s

Table 3 *Definition of Earth ellipsoid parameters and setting of appropriate values according to the WGS-84 model.*

2.2.1 *Short-term error mechanisms and analysis (ψ-angle error approach) of IMU accuracy in positioning*

For the purpose of **error analysis**, the navigation system can be viewed as attempting solutions of the navigation equations in position, linear speed and attitude with respect to either a *computer* frame, c (according to the ψ-angle error approach), or a *true* frame, t (according to the perturbation error approach). Both these frames correspond to particular r frames and are assumed to nominally coincide with the local level navigation frame l. The error analysis is assessed according to the ψ-angle error approach [5] which is proved to be equivalent to the perturbation error analysis, which in turn is more intuitive, but implies more complicated error equations because of the presence of higher number of terms. The computer frame c is defined as the "corrupted" version of the local level frame l as computed by the navigation system.

For SAS applications it is necessary to evaluate over a SASIT period the error in sonar position displacement with respect to the aperture beginning, $\delta\vec{p}_{es}$. The sonar phase centre is selected as sonar reference point S. The sonar position displacement error consists of the sum of the body position displacement error as computed by the navigation system and the error in measuring/computing the lever arm between S and the navigation system reference point B (which is assumed to coincide with the body frame origin):

$$\delta\vec{p}_{es} = \delta\vec{p}_{eb} + \delta\vec{L}_{bs}. \tag{16}$$

IMU Platform position error

According to the ψ-angle error analysis, for small error angles and under the hypothesis, generally accepted, of exact knowledge of the quantities $\omega^c_{ic} = \omega^c_{il}$, $\omega^c_{ec} = \omega^c_{el}$, ω^c_{ie} and C^c_e, the error equations of platform (i.e., body) position, linear speed and

attitude, referred to the Earth and decomposed in the computer frame, are [1][5][4]:

$$\begin{aligned}
\delta\dot{\mathbf{p}}^c_{eb} &= -\omega^c_{ec} \wedge \delta\mathbf{p}^c_{eb} + \delta\mathbf{v}^c_{eb} \\
\delta\dot{\mathbf{v}}^c_{eb} &= \mathbf{f}^c_{ib} \wedge \psi^c_{cb} + \delta\mathbf{g}'^c_{ib} - (2\omega^c_{ie} + \omega^c_{ec}) \wedge \delta\mathbf{v}^c_{eb} + \delta\mathbf{f}^c_{ib} \\
\dot{\psi}^c_{cb} &= -(\omega^c_{ie} + \omega^c_{ec}) \wedge \psi^c_{cb} - \delta\omega^c_{ib}
\end{aligned} \tag{17}$$

where:
$\delta\mathbf{p}^c_{eb}$ and $\delta\mathbf{v}^c_{eb}$ are the IMU navigation position and velocity errors respectively, decomposed in the c frame,
ψ^c_{cb} is the vector of misalignment angles between the body frame b and computed c navigation frame (being a misalignment vector the angles are supposed small),
$\delta\mathbf{g}'^c_{ib}$ is the error in the gravity vector as seen in the computer frame,
ω^c_{ec} is the transport rate vector of the navigation frame with respect to the Earth, as seen from the navigation frame (being null in the case of a computer frame fixed re. the Earth),
$\delta\mathbf{f}^c_{ib}$ and $\delta\omega^c_{ib}$ are the accelerometer and gyro sensor errors respectively as seen from the computer frame.

Over a SASIT interval, lasting from 10 to 100 seconds in typical applications, this model is simplified. Variables are defined as the sum of their value at the SASIT start, indicated with the instant t_0, plus their changes with time:

$$\psi^c_{cb} = \psi_0 + \Delta\psi^c_{cb} \tag{18}$$

(all the variables with the subscript "0" are referred to the time instant t_0). At short term, the following hypotheses are formulated: the accelerations along a SAS aperture (performed along a straight line path of the vehicle trajectory at nominal constant speed) are expected to be small; the Coriolis effect and the transport rate (which here is identically null being the l_0 frame fixed re. the Earth) are assumed to be negligible; the gravity error is assumed to be constant over the whole SASIT and equal to the value in t_0 (i.e., $\delta\mathbf{g}'^c_{ib} = \delta\mathbf{g}'_0$). Finally only the IMU sensor errors as seen in the body frame are available, hence their transformation between b and c frame is needed (i.e., $\delta\mathbf{f}^c_{ib} = C^c_b\delta\mathbf{f}^b_{ib}$, $\delta\omega^c_{ib} = C^c_b\delta\mathbf{f}^b_{ib}$).

Under these hypotheses the set of equations (17), approximated at the first order, becomes:

$$\begin{aligned}
\delta\dot{\mathbf{p}}^c_{eb} &= \delta\mathbf{v}^c_{eb} \\
\delta\dot{\mathbf{v}}^c_{eb} &= \mathbf{f}^c_{ib} \wedge \psi_0 - \mathbf{g}^c_{ib} \wedge \Delta\psi^c_{cb} + \delta\mathbf{g}'_0 + C^c_b\delta\mathbf{f}^b_{ib} \\
\dot{\psi}^c_{cb} &= \Delta\dot{\psi}^c_{cb} = -\omega^c_{ie} \wedge \psi^c_{cb} - C^c_b\delta\omega^b_{ib}
\end{aligned} \tag{19}$$

As aforesaid, we are interested in the error in position displacement relative to the aperture beginning, computed along a SASIT period. This can be obtained from the navigation equations above by integration of accelerations and velocities. Integration must be computed in a frame remaining fixed with time. To this aim,

although over an aperture the local level changes are negligible, in order to follow a rigorous approach, we decide to select as c the *initial* local level frame l_0, that is the Earth-fixed local frame centred on the vertical of the position occupied by the body at the SASIT beginning t_0. The l_0 frame is sketched in Annex A, where it is also related to the current l frame (centred on the vertical of the body position at the present time t within the SASIT).

Now, as described in Annex B, by integration between the aperture initial time t_0, set to 0 without lack of generality, and the generic time t within the SASIT, the approximated short-term IMU position and angle misalignment displacement errors in the computed l_0 frame, c, become:

$$\begin{array}{ll} \delta\mathbf{p}^c_{eb} = & (\mathbf{p}^c_{eb} - \mathbf{v}_0 t) \wedge \psi_0 + \delta\mathbf{v}_0 t + \left(\delta\mathbf{g'}_0 - \mathbf{g}^{l_0}_{ib} \wedge \psi_0\right) \frac{t^2}{2} + \\ & + \mathbf{g}^{l_0}_{ib} \wedge (\omega^c_{ie} \wedge \psi_0) \frac{t^3}{6} + \delta\mathbf{p}^c_\omega + \delta\mathbf{p}^c_a \\ \Delta\psi^c_{cb} = & -(\omega^c_{ie} \wedge \psi_0)\, t - \int_0^t C^c_b \delta\omega^b_{ib} d\tau, \end{array} \tag{20}$$

where $\delta\mathbf{p}^c_a$ and $\delta\mathbf{p}^c_\omega$ are the position displacement errors due to the accelerometer and gyro errors respectively, defined as:

$$\begin{array}{l} \delta\mathbf{p}^c_a = \int\int C^c_b \delta\mathbf{f}^b_{ib} d\tau d\tau' \\ \delta\mathbf{p}^c_\omega = \mathbf{g}^{l_0}_{ib} \wedge \int\int\int C^c_b \delta\omega^b_{ib} d\tau d\tau' d\tau'' \end{array} \tag{21}$$

The IMU errors are modelled in a more or less accurate way depending on the detail in the sensor specifications provided by the constructor.

Taking into account the standard parameters usually available from a constructor of high quality systems, the **accelerometer error** $\delta\mathbf{f}^b_{ib}$ is modelled as follows:

$$\delta\mathbf{f}^b_{ib} = \mathbf{\Delta} + A\mathbf{f}^b_{ib} + N_a(\mathbf{f}^b_{ib})^2 + \eta_a, \tag{22}$$

where:

$\mathbf{\Delta}$ is the accelerometer bias repeatability, which is generally modelled with a Markov process of the first order. However, being the time constant of the Markov process usually much bigger than a typical SASIT period, $\mathbf{\Delta}$ can be considered time invariant.

A is the accelerometer constant scale factor matrix:

$$A = \begin{bmatrix} \delta s_{a,x} & 0 & 0 \\ \gamma_{a,yz} & \delta s_{a,y} & 0 \\ \gamma_{a,zy} & \gamma_{a,zx} & \delta s_{a,z} \end{bmatrix}, \tag{23}$$

where $\delta s_{a,i}$ $(i = x, y, z)$ are the accelerometer scale factor errors and $\gamma_{a,ij}$ $(i, j = x, y, z)$ are the nonorthogonality angles of the input axis i with respect to axis j.

The matrix A is lower triangular as the accelerometer x axis is assumed to coincide with the body frame x axis.

N_a is the accelerometer constant scale factor nonlinearity matrix:

$$N_a = \frac{1}{2}\begin{bmatrix} \delta n_{a,x} & 0 & 0 \\ 0 & \delta n_{a,y} & 0 \\ 0 & 0 & \delta n_{a,z} \end{bmatrix}, \tag{24}$$

where $\delta n_{a,i}$ are the scale factor nonlinearities.

Finally η_a is the vector of white noise.

By expressing the accelerometer error in terms of the sensor error parameters, the position displacement error due to the accelerometer becomes:

$$\delta \mathbf{p}_a^c = \int\int C_b^c \left(\boldsymbol{\Delta} + A\mathbf{f}_{ib}^b + N_a(\mathbf{f}_{ib}^b)^2 + \eta_a\right) d\tau d\tau' \tag{25}$$

The hypotheses of good vehicle stabilization and small misalignment angles between l_0 and c frames over an aperture are assumed. Hence by expressing the force $\mathbf{f}$ in terms of acceleration and mass attraction (the latter assumed to be constant over the SASIT time), the position displacement error due to the accelerometer, approximated at the first order, is:

$$\begin{aligned} \delta \mathbf{p}_a^c \approx \; & \boldsymbol{\Delta}' \tfrac{t^2}{2} + C_{b_0}^c A \int\int \mathbf{a}_{ib}^b d\tau d\tau' + C_{b_0}^c N_a \int\int \left(\left(\mathbf{a}_{ib}^b\right)^2 - 2\mathbf{a}_{ib}^b \mathbf{g}_{ib}^b\right) d\tau d\tau' + \\ & + \int\int C_b^c \eta_a d\tau d\tau', \end{aligned} \tag{26}$$

where b_0 is the body frame at t_0 and now the time-invariant bias term $\boldsymbol{\Delta}'$ contains not only the accelerometer bias but also terms depending on the gravitational field:

$$\boldsymbol{\Delta}' = C_{b_0}^c \left(\boldsymbol{\Delta} + A\mathbf{g}_{ib}^{l_0} + N_a(\mathbf{g}_{ib}^{l_0})^2\right). \tag{27}$$

Notice that if g is the Earth mass attraction magnitude, assumed time invariant over a SASIT period, $\mathbf{g}_{ib}^{l_0}$ is expressed as:

$$\mathbf{g}_{ib}^{l_0} = [0 \;\; 0 \;\; g]^T, \tag{28}$$

which is computationally very convenient.

The **gyro error** $\delta\omega_{ib}^b$ is modelled as:

$$\delta\omega_{ib}^b = \epsilon + \Gamma\omega_{ib}^b + N_\omega(\omega_{ib}^b)^2 + \eta_\omega, \tag{29}$$

where:

ϵ is the gyro bias repeatability. The same consideration as stated for the accelerometer bias can be applied; hence ϵ can be assumed to be time-invariant over a SASIT period.

Γ is the gyro scale factor error matrix, which is time invariant:

$$A = \begin{bmatrix} \delta s_{\omega,x} & \gamma_{\omega,xz} & \gamma_{\omega,xy} \\ \gamma_{\omega,yz} & \delta s_{\omega,y} & \gamma_{\omega,yx} \\ \gamma_{\omega,zy} & \gamma_{\omega,zx} & \delta s_{\omega,z} \end{bmatrix}, \tag{30}$$

where $\delta s_{\omega,i}$ $(i = x, y, z)$ are the gyro scale factor errors and $\gamma_{\omega,ij}$ $(i, j = x, y, z)$ are the nonorthogonality angles of the input axis i with respect to axis j.

N_ω is the matrix of gyro constant scale factor nonlinearity errors:

$$N_\omega = \frac{1}{2} \begin{bmatrix} \delta n_{\omega,x} & 0 & 0 \\ 0 & \delta n_{\omega,y} & 0 \\ 0 & 0 & \delta n_{\omega,z} \end{bmatrix}, \tag{31}$$

where $\delta n_{\omega,i}$ are the scale factor nonlinearities.

Finally η_ω is the gyro angular random walk.

By expressing the gyro error in terms of the sensor error parameters, the position displacement error due to the gyro becomes:

$$\delta \mathbf{p}_\omega^c = \left(\mathbf{g}_{ib}^{l_0} \wedge\right) \int\int\int C_b^c \left(\epsilon + \Gamma \omega_{ib}^b + N_\omega (\omega_{ib}^b)^2 + \eta_\omega\right) d\tau d\tau' d\tau''. \tag{32}$$

Under the same assumptions as adopted for accelerometer error analysis, the position displacement error due to the gyro approximated at the first order becomes:

$$\begin{aligned} \delta \mathbf{p}_\omega^c \approx & \left(\mathbf{g}_{ib}^{l_0} \wedge C_{b_0}^c \epsilon\right) \frac{t^3}{6} + \mathbf{g}_{ib}^{l_0} \wedge C_{b_0}^c \Gamma \int\int\int \omega_{ib}^b d\tau d\tau' d\tau'' + \\ & + \mathbf{g}_{ib}^{l_0} \wedge C_{b_0}^c N_\omega \int\int\int (\omega_{ib}^b)^2 d\tau d\tau' d\tau'' + \mathbf{g}_{ib}^{l_0} \wedge \int\int\int C_b^c \eta_\omega d\tau d\tau' d\tau''. \end{aligned} \tag{33}$$

2.2.2 *Lever arm error and sonar-IMU angle misalignment error*

The sonar phase centre, which is assumed to be the origin of the sonar body frame, S, is located in a different point of the vehicle with respect to the IMU body frame origin, B. The consequent lever arm $\mathbf{L}_{bs}$ between the IMU body frame origin and the sonar phase centre which must be precisely measured and decomposed in the c frame, follows the dynamic equation:

$$\dot{\mathbf{L}}_{bs}^c = C_b^c \left(\omega_{lb}^b \wedge \mathbf{L}_{bs}^b\right) + C_b^c \dot{\mathbf{L}}_{bs}^b. \tag{34}$$

In order to estimate the measurement errors, perturbation analysis is applied and the lever arm correction error approximated at the first order results to be:

$$\begin{aligned} \delta \mathbf{L}_{bs}^c &= \int_{t_0}^t \delta \left(C_b^c \left(\omega_{lb}^b \wedge \mathbf{L}_{bs}^b\right)\right) d\tau = \\ &= \int_{t_0}^t \delta C_b^c \left(\omega_{lb}^b \wedge \mathbf{L}_{bs}^b\right) d\tau + \int_{t_0}^t C_b^c \left(\delta \omega_{lb}^b \wedge \mathbf{L}_{bs}^b\right) d\tau + \int_{t_0}^t C_b^c \left(\omega_{lb}^b \wedge \delta \mathbf{L}_{bs}^b\right) d\tau \end{aligned} \tag{35}$$

Among the three terms, depending respectively on body misalignment errors, body angular rate errors and lever arm errors, only the third is considered significant, the other two being infinitesimal of second order, hence negligible, due to vehicle stabilization. Hence, assumed $t_0 = 0$ as in Section 2.2.1, we obtain:

$$\delta \mathbf{L}^c_{bs} \approx \int_0^t C^c_b \left(\omega^b_{lb} \wedge \delta \mathbf{L}^b_{bs} \right) d\tau. \tag{36}$$

The sonar array and the IMU platform are oriented in such a way that the sonar reception beam is perpendicular to the IMU body frame x axis. Hence the body and sonar frame axes directions ideally coincide apart from the roll angle ϕ_{bs} of which the sonar frame is rolled for impinging a certain area of the sea bottom. This roll angle can be assumed to be constant over a SASIT and equal to the value assumed in t_0. However, because of boresighting errors, the IMU body frame is also expected to be misaligned with respect to the sonar body frame by a constant and typically small vector ψ_{bs}.

Now, called $\delta \mathbf{p}^c_{es}$ the error in sonar position displacement along a SAS aperture re. the aperture beginning, and $\Delta\psi^c_{cs}$ the change in the sonar angle misalignment along an aperture re. the aperture beginning, both decomposed in the c frame, these two error quantities can be expressed as:

$$\begin{aligned} \delta \mathbf{p}^c_{es} = \quad & (\mathbf{p}^c_{eb} - \mathbf{v}_0 t) \wedge \psi_0 + \delta \mathbf{v}_0 t + \left(\delta \mathbf{g'}_0 - \mathbf{g}^{l_0}_{ib} \wedge \psi_0 \right) \tfrac{t^2}{2} + \mathbf{g}^{l_0}_{ib} \wedge (\omega^c_{ie} \wedge \psi_0) \tfrac{t^3}{6} + \\ & + \delta \mathbf{p}^c_{\omega} + \delta \mathbf{p}^c_a + \delta \mathbf{L}^c_{bs} \\ \Delta\psi^c_{cs} = \quad & \Delta\psi^c_{cb} = -(\omega^c_{ie} \wedge \psi_0)\, t - \textstyle\int_0^t C^c_b \delta\omega^b_{ib} d\tau. \end{aligned} \tag{37}$$

where the IMU sensor error terms, the lever-arm error and the IMU body angle misalignment are expressed according to Eqs (26), (33), (36) and (20) respectively.

2.2.3 Position displacement error. Discussion

If the error analysis is limited to the sonar position displacement over a SASIT, the following considerations can be drawn.

The expression of the sonar position displacement error of Eq. (37) can be rearranged as:

$$\delta \mathbf{p}^c_{es} = \mathbf{T}_0 + \mathbf{T}_{1,a} + \mathbf{T}_{1,\omega} + \mathbf{T}_{2,a} + \mathbf{T}_{2,\omega} + \mathbf{T}_{3,a} + \mathbf{T}_{3,\omega}, \tag{38}$$

where the "T" terms are defined as:

$$
\begin{aligned}
\mathbf{T}_0 = &\quad (\psi_0 \wedge \mathbf{v}_0 + \delta\mathbf{v}_0)t, \\
\mathbf{T}_{1,a} = &\quad \left(\delta\mathbf{g}'^c_0 - \mathbf{g}^{l_0}_{ib} \wedge \psi_0 + \boldsymbol{\Delta}'\right)\frac{t^2}{2}, \\
\mathbf{T}_{1,\omega} = &\quad \mathbf{g}^{l_0}_{ib} \wedge \left(C^c_{b_0}\epsilon + \omega^c_{ie} \wedge \psi_0\right)\frac{t^3}{6}, \\
\mathbf{T}_{2,a} = &\quad \mathbf{p}^c_{eb} \wedge \psi_0 + C^c_{b_0} A \int\int \mathbf{a}^b_{ib} d\tau d\tau' + C^c_{b_0} N_a \int\int \left(\left(\mathbf{a}^b_{ib}\right)^2 - 2\mathbf{a}^b_{ib}\mathbf{g}^b_{ib}\right) d\tau d\tau', \\
\mathbf{T}_{2,\omega} = &\quad \mathbf{g}^{l_0}_{ib} \wedge \left(C^c_{b_0}\Gamma \int\int\int \omega^b_{ib} d\tau d\tau' d\tau'' + C^c_{b_0} N_\omega \int\int\int (\omega^b_{ib})^2 d\tau d\tau' d\tau''\right) + \\
&\quad + \int_{t_0}^{t} C^c_b \left(\omega^b_{lb} \wedge \delta\mathbf{L}^b_{bs}\right) d\tau, \\
\mathbf{T}_{3,a} = &\quad \int\int C^c_b \eta_a d\tau d\tau', \\
\mathbf{T}_{3,\omega} = &\quad \mathbf{g}^{l_0}_{ib} \wedge \int\int\int C^c_b \eta_\omega d\tau d\tau' d\tau''.
\end{aligned}
\tag{39}
$$

The $\mathbf{T}$ term contributions are considered separately.

Error contribution from $\mathbf{T}_0$

The $\mathbf{T}_0$ term varies linearly with time according to a constant coefficient that depends only on attitude misalignment (through ψ_0) and velocity computation error at the start of the aperture. It does not depend on IMU sensor measurement errors, hence it is of limited interest for IMU quality evaluation.

Error contribution from $\mathbf{T}_{1,a}$ *and* $\mathbf{T}_{1,\omega}$

The $\mathbf{T}_{1,a}$ and $\mathbf{T}_{1,\omega}$ terms are polynomial functions in time the approximately constant coefficients of which depend on alignment (through ψ_0) and bias errors (inertial sensor biases $\boldsymbol{\Delta}'$ and ϵ, and gravity anomaly $\delta\mathbf{g}'^c_0$) at the start of an aperture. That the major source of position displacement error is due to acceleration bias [1] is confirmed by the simulation presented in Section 3. Acceleration bias is the sum of gravity anomaly ($\delta\mathbf{g}'^c_0$), accelerometer bias ($\boldsymbol{\Delta}'$) and gravitational field misresolved by the horizontal angle misalignments ($\mathbf{g}^{l_0}_{ib} \wedge \psi_0 = g\,[-\psi_{0,y},\ \ \psi_{0,x},\ \ 0]^T$). Among these three components the accelerometer bias usually gives the most significant contribution.

If the system undergoes stationary alignment (i.e., at constant speed and with no turns), the only angular rate sensed by the IMU is the Earth rate, having zero East component in principle. The only acceleration sensed by the IMU is the gravity force, which is assumed to have non-zero Down component only. As a consequence, during this phase the horizontal misalignments are correlated with the accelerometer bias and gravity anomaly, so that:

$$\boldsymbol{\Delta}' + \delta\mathbf{g}'^c_0 \approx \mathbf{g}^{l_0}_{ib} \wedge \psi_0. \tag{40}$$

The Earth rate misresolved by attitude error (i.e., the angle misalignment between b and l_0), and in particular by heading error (i.e., the z-component of this misalignment) is correlated to, hence can be compensated by, the gyro bias:

$$C_{b_0}^{c}\epsilon \approx \psi_0 \wedge \omega_{ie}^{c}. \tag{41}$$

The two $\mathbf{T}_1$ error terms become significant during (and hence, immediately after) vehicle turns, when the acceleration bias is uncorrelated with the x and y components of angle misalignments and the gyro bias is uncorrelated with ω_{ie}^{c} $(= \omega_{ie}^{l_0})$. As detailed in [1], this is formally expressed by the following formulas for the position displacement error variances due to $\mathbf{T}_{1,a}$ and $\mathbf{T}_{1,\omega}$ respectively:

$$\begin{aligned}
\sigma_{p,1a}^2 &\approx \left(\begin{bmatrix} 1 & 0 \\ 1 & 0 \\ 1 & g^2 \end{bmatrix} \begin{bmatrix} \sigma_{\Delta}^2 \\ \sigma_{\delta s_{a,z}}^2 \end{bmatrix} + \begin{bmatrix} g^2 & 0 \\ 0 & g^2 \\ 0 & 0 \end{bmatrix} \begin{bmatrix} \sigma_{\psi_y}^2 \\ \sigma_{\psi_z}^2 \end{bmatrix} \right) \frac{t^4}{4}, \\
\sigma_{p,1\omega}^2 &\leq \left(\begin{bmatrix} g^2 \\ g^2 \\ 0 \end{bmatrix} \sigma_{\epsilon}^2 + \begin{bmatrix} g^2\Omega^2 & 0 & g^2\Omega^2 \\ 0 & g^2\Omega^2 & 0 \\ 0 & 0 & 0 \end{bmatrix} \begin{bmatrix} \sigma_{\psi_x}^2 \\ \sigma_{\psi_y}^2 \\ \sigma_{\psi_z}^2 \end{bmatrix} \right) \frac{t^6}{36},
\end{aligned} \tag{42}$$

where σ_{Δ}^2, $\sigma_{\delta s_{a,z}}^2$, σ_{ϵ}^2, $\sigma_{\psi_x}^2$, $\sigma_{\psi_y}^2$, $\sigma_{\psi_z}^2$ are the variances respectively of accelerometer bias (assumed constant over the three components), z-component of the accelerometer linear scale factor error, gyro bias (assumed constant over the three components), and x-, y- and z-component angle misalignment. While rigorously the IMU sensor errors should all be referred to the c frame, a good approximation is achieved by assuming them to be referred to the b frame under the hypothesis of small angles. The scale factor non linearities and the gravity anomalies are neglected here.

As a consequence, the displacement error standard deviation due to the accelerometer bias $\mathbf{\Delta}'$ varies in time with t^2, while that due to the gyro bias ϵ varies with t^3.

Error contribution from $\mathbf{T}_{2,a}$ *and* $\mathbf{T}_{2,\omega}$

The $\mathbf{T}_2$ terms contain the coupling of the dynamic vehicle variables (in particular body acceleration and angular rate) and the lever arm error with the inertial sensor errors (in particular, scale factor linear and non linear errors and non-orthogonality errors). Actually, only the random components of the acceleration and the angular rate sensed by the body contribute to the position displacement error variance, not the dynamic components attributable to vehicle motion imposed by the user and hence are deterministic. For AUVs these random components are attributable to waves and underwater currents.

The theoretical evaluation of these components in the case of a ROV (in which case random accelerations and angular rates are applied because of periodic tow-

cable forces induced by waves to the mothership motion) is formalized in [1] where appropriate dynamic assumptions are introduced. The conclusions deduced in [1] are that a high-quality IMU should provide sufficiently small scale factor and non-orthogonality errors to be compliant with the most stringent accuracy contraints, while the most significant, and so critical, error component should remain the lever arm correction error. Further according to the example proposed in [1], for a global error budget in terms of $\lambda/16$ fixed to 1.25 mm (corresponding to a sonar central frequency of 75 kHz) should be kept in the order of 1 cm.

On the basis of the available NavLab simulator, neither the dynamic random variables of the vehicle motion nor the lever arm and its error can be realistically modelled [4]. Hence the contribution to error from the $\mathbf{T}_2$ terms cannot be evaluated. More detailed and precise error evaluation measurements (under controlled conditions) of the motion of the AUV recently procured by SACLANTCEN will contribute to realistic modelling of these random contributions and hence, their computation in an extended version of the navigational simulator.

Error contribution from $\mathbf{T}_{3,a}$ *and* $\mathbf{T}_{3,\omega}$

The $\mathbf{T}_{3,a}$ and $\mathbf{T}_{3,\omega}$ terms represent the contributions to position displacement error due to accelerometer and gyro white noise respectively. As shown in [1], assumed the sensor white noise components as Gaussian and reciprocal uncorrelated, it is straightforward to derive the respective variances of position error contributions as:

$$\begin{aligned} \sigma^2_{p,3a} &= [q_{\eta_a,x}, \quad q_{\eta_a,y}, \quad q_{\eta_a,z}]^T \frac{t^3}{6}, \\ \sigma^2_{p,3\omega} &= [q_{\eta_\omega,y}, \quad q_{\eta_\omega,x}, \quad 0]^T \frac{g^2 t^5}{120}, \end{aligned} \tag{43}$$

where rigorously the q terms are the spectral densities of the accelerometer and gyro white noise components referred to the c frame. As for the previous term analysis, under the hypothesis of small angle misalignment, they correspond with good approximation to the spectral density values provided by the constructor (i.e., refered to the b frame).

As a consequence, the displacement error standard deviation due to accelerometer random noise η_a is shown to vary in time with $t^{3/2}$, that due to gyro random noise η_ω with $t^{5/2}$.

Even in the case that the INS is aided by other navigation sensors and an EKF approach is used for data fusion and navigation accuracy improvement, the IMU white noise components cannot be filtered out at short term. However for high-quality IMUs the spectral density of the gyro white noise is generally sufficiently small to be acceptable [1]. Analogously, the white noise of the IMU accelerometers must be requested to be low as a critical sensor specification. In Section 3 the effects

and levels of these two error contributions will be shown and compared for the high quality sensor procured by SACLANTCEN.

2.2.4 *Displacement of attitude misalignment. Discussion*

The error analysis of the sonar attitude displacement re. the aperture beginning (ψ^c_{cs}) is considered now. The error expression of Eq. (37) can be rearranged as:

$$\Delta\psi^c_{cs} = \mathbf{P}_{1,\omega} + \mathbf{P}_{2,\omega} + \mathbf{P}_{3,\omega}, \tag{44}$$

where the "**P**" terms are defined as:

$$\begin{aligned} \mathbf{P}_{1,\omega} &= -\left(C^c_{b_0}\epsilon + \omega^c_{ie} \wedge \psi_0\right) t, \\ \mathbf{P}_{2,\omega} &= -C^c_{b_0}\Gamma \int_0^t \omega^b_{ib} d\tau - C^c_{b_0} N_\omega \int_0^t (\omega^b_{ib})^2 d\tau, \\ \mathbf{P}_{3,\omega} &= -\int_0^t C^c_b \eta_\omega d\tau. \end{aligned} \tag{45}$$

The **P** term contributions are considered separately as follows.

Error contribution from $\mathbf{P}_{1,\omega}$

The $\mathbf{P}_{1,\omega}$ is approximated with a polynomial function of the first order in time, the roughly constant coefficient of which depends on alignment errors (through ψ_0) and gyro bias error ϵ at the start of an aperture. Hence the same considerations as drawn for the position error $T_{1,\omega}$ term are applicable here.

During stationary alignment phases the Earth rate misresolved by attitude error is correlated to, hence can be compensated by, the gyro bias according to Eq. (41). As explained in Section 2.2.3, the $\mathbf{P}_{1,\omega}$ error term becomes significant during (and hence, immediately after) vehicle turns, when the gyro bias is uncorrelated with ω^c_{ie}. This is formally represented by the following expression for $\mathbf{P}_{1,\omega}$ variance:

$$\sigma^2_{\psi,1\omega} \leq \left(\begin{bmatrix} 1 \\ 1 \\ 1 \end{bmatrix} \sigma^2_\epsilon + \begin{bmatrix} 0 & \Omega^2 & 0 \\ \Omega^2 & 0 & \Omega^2 \\ 0 & \Omega^2 & 0 \end{bmatrix} \begin{bmatrix} \sigma^2_{\psi_x} \\ \sigma^2_{\psi_y} \\ \sigma^2_{\psi_z} \end{bmatrix} \right) t^2, \tag{46}$$

Hence, the attitude displacement error standard deviation due to the gyro bias ϵ varies with t.

Error contribution from $\mathbf{P}_{2,\omega}$

The $\mathbf{P}_{2,\omega}$ term contains the coupling of the vehicle angular rate with gyro scale factor linear and non linear errors and non-orthogonality errors. Analogously to the position error $\mathbf{T}_2$ components, only the random components of the angular rate sensed by the body contribute to $\mathbf{P}_{2,\omega}$ error variance. In the present NavLab version, these random components cannot be simulated/estimated, hence the $\mathbf{P}_{2,\omega}$ term cannot be discussed here, but for high-quality IMU sensors $\mathbf{P}_{2,\omega}$ contribution to global error is expected to be negligible [1].

Error contribution from $\mathbf{P}_{3,\omega}$

The $\mathbf{P}_{3,\omega}$ term represents the contribution to attitude displacement error due to gyro white noise η_ω. As derived in Section 2.2.3, it is assumed that the sensor white noise components are Gaussian and reciprocally uncorrelated, hence the $\mathbf{P}_{3,\omega}$ variance is:

$$\sigma^2_{\psi,3\omega} = [q_{\eta_\omega,x}, \quad q_{\eta_\omega,y}, \quad q_{\eta_\omega,z}]^T \, t. \tag{47}$$

As discussed with reference to Eq. (43), if the q terms are the gyro white noise spectral densities referred to the c frame, the equation above is exact, but a good approximation is achieved by using the corresponding spectral density values referred to the b frame and provided by the IMU constructor.

We can notice that the displacement error standard deviation due to the gyro random noise varies with $\sqrt{t}$. This result could be easily forecast as this angle error contribution comes from the integration of white noise, i.e., is a random walk process [6].

3

INS error analysis based on simulation

In this chapter the validation of the theoretical considerations drawn in Section 2 is addressed by simulation. This allows the evaluation of short-term position and orientation accuracy achievable by means of an INS system rigidly installed with the sonar array on an underwater vehicle. The comparison of the forecast estimation accuracy with the requirements imposed for guaranteeing SAS image quality is outlined.

The quantification of the error affecting the position and attitude displacements of the sonar along a SAS integration time (i.e., by short-term analysis) is performed in terms of main contributions of sensor measurement errors on the basis of simulated data analysis.

3.1 Test procedure for error statistical analysis

The error analysis purpose is to statistically evaluate the position and attitude displacement errors over the time window of an aperture (i.e., over a SASIT) with respect to the accuracy constraints imposed by the selected SAS application.

To perform SAS, a sonar aperture consisting of multiple transducers assembled in a rigid frame is mounted on a stable underwater vehicle. The transducer signals are continuously acquired and processed over a sliding time window, corresponding to a SASIT period. The acoustic wavelength, the SASIT length, and the rate of update of the related time window, known as the pulse repetition frequency (PRF), depend on the application.

Given the sonar central wavelength λ and the sonar array length L_a, the AINS is required to provide navigational estimates of the sonar phase centre during an aperture with a maximum tolerated error of $\lambda/16$ on position displacement and of $\lambda/(8L_a)$ on attitude displacement.

In order to give typical values of these thresholds in the case of common SAS applications, three examples are selected here:

- hunting of buried mines by means of Low Frequency (LF) sonar;

- hunting of proud mines by means of High Frequency (HF) sonar;
- seabed survey at intermediate frequencies.

In the first case the sonar central frequency is set to 10 kHz, in the second case the central frequency of the sonar is set to 300 kHz, in the last case the central frequency is supposed to be 50 kHz.
On the basis of main sonar and SAS parameters characterizing the three pilot applications the corresponding error thresholds can be computed, as summarized in Table 4.

SAS Parameter	LF sonar (buried mines)	HF sonar (proud mines)	Survey sonar
Wavelength λ (cm)	15.00	0.5	3
Min. array length L_a (m)	0.06	0.8	4
SAS Length L (m)	22.50	20.0	15
SASIT (s)	15.00	14.0	10
Position error threshold $\frac{\lambda}{16}$(cm)	1	0.030	0.200
Attitude error threshold $\frac{\lambda}{8L_a}(^o)$	18	0.045	0.054

Table 4 *Definition and value of the main SAS parameters and related constraints for three pilot applications.*

The test procedure is shown in Fig. 1. The navigational simulator/estimator NavLab was developed and provided to SACLANTCEN by NDRE (Norwegian Defence Research Establishment) [4] (Annex C). The capabilities of NavLab include navigational sensor data simulation, IMU navigation equation solution and KF-based data integration and navigation estimation from various types of sensor data. This report is limited to:

- on the basis of a selected test configuration, simulation of the ideal (i.e., true) values of all the vehicle dynamic variables involved in navigation (namely, geographic position and orientation, linear and angular velocities and accelerations of the vehicle) as time varies, i.e, along the specified trajectory;
- simulation of sensor main error contributions on the basis of the IMU sensor specifications;
- from the combination of the first two results, simulation of the outputs measured by the selected IMU (i.e., inertial force and angular rate);
- solution of the strapdown navigation equations using as inputs the simulated measurements. It corresponds to the navigation result in free-inertial mode in terms of vehicle position, attitude and velocity computation. The comparison

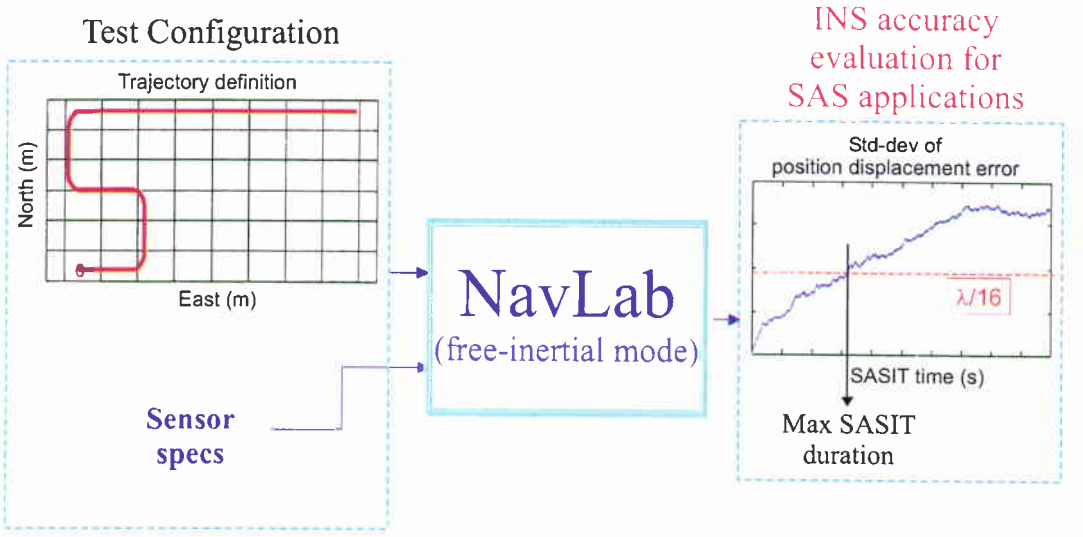

Figure 1 *Scheme of test procedure for error statistical analysis.*

between the navigator outputs and the true corresponding quantities allows the evaluation of the system error.

For a selected test configuration, a set of runs are performed so that a statistical analysis in terms of the values and changes with time of error standard deviation along a SAS aperture can be obtained. The standard deviation values of position and attitude errors can be compared with the error thresholds imposed by SAS accuracy requirements for a certain application, so that the maximum SASIT duration can be estimated and compared with that effectively required by that application (see Table 4).

In a more detailed error analysis, by means of the simulation results it is also possible to perform a statistical evaluation of the main error contributions of the IMU sensor separately. This allows one to select/specify the IMU having the most suitable performance characteristics for achieving the accuracy requirements of a certain SAS application, and to focus the efforts in improving the design of an integration/estimation architecture on the reduction of the error components which most influence the positioning performance in SAS applications.

3.2 Definition of test configuration

The IMU selected for tests recently procured by SACLANTCEN is produced by iMAR. It is a high-quality sensor consisting of a 3-axes laser gyro (Honeywell GG1320) and three accelerometers (Honeywell QA2000). The main error parameters

of the sensor provided by the constructor are summarized in Table 5. These values are used as inputs to Navlab simulator in order to generate appropriate random processes of measurement errors. The bias errors are simulated as Markov processes of the first order with the specified standard deviation and a long time constant set to 1800s [4][6]. The white noise processes are assumed to be Gaussian [4].

Error Parameter	Unit	Value
Gyro (each axis)		
Bias Repeatability (std-dev)	$(^o/hr)$	0.003
Scale Factor error (std-dev)	pure number	10 ppm
Scale Factor nonlinearity (std-dev)	pure number	10 ppm
White Noise (power density)	$(^o/\sqrt{hr})$	0.003
Accelerometer (each axis)		
Bias Repeatability (std-dev)	(μg)	30
Scale Factor error (std-dev)	pure number	70 ppm
Scale Factor nonlinearity (std-dev)	$(\mu g/g^2)$	15
White Noise (power density)	$(\mu g/\sqrt{Hz})$	8

Table 5 *Definition and value of the main error parameters of iMAR IMU sensor.*

The simulated true trajectory selected for statistical tests is shown in Fig. 2 on the plane (NE) defined by the fixed local level frame centred in the trajectory starting point O. The trajectory is typical of an AUV survey mission. The SAS processing is generally performed along straight line paths, in this case along the final 200 m segment, which is bounded in the plot by the points indicated as t_0 and t_1, corresponding to the first and last time instant of the aperture period.

The vehicle is supposed to travel at a constant depth of 20 m, at the constant speed of 2 m/s, with a constant angular rate of 15 °/s during turns. Under these conditions the SASIT period along the last 200 m of the trajectory is 100 s. The mission is supposed to start in a sea area close to La Spezia, at the initial geographic coordinates (44° latitude, 10° longitude), heading East.

3.3 Simulation results

The statistical analysis of the error in position and attitude displacements along a SAS aperture with respect to the SAS starting point is performed by using the IMU sensor only, i.e., under free-inertial navigation conditions. It is based on a relatively large number of runs (i.e., 150) of the Navlab simulator described in Annex C.

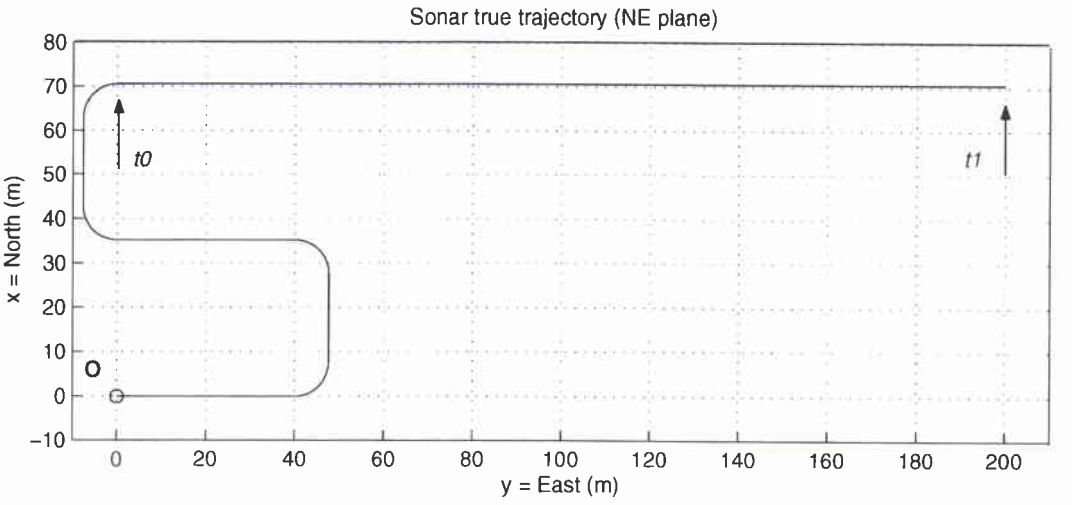

Figure 2 *Simulated true trajectory of the sonar (hence of the body) selected for sensor accuracy tests. The trajectory is seen from a fixed local level frame centred in the mission starting point O and projected on its North-East horizontal plane.*

3.3.1 Simulated position errors

The statistical analysis presented is performed on the basis of 150 runs of the Navlab simulator under the same test configuration.

In Fig. 3 the standard deviation computed on 150 runs of the global position displacement error as expressed in Eq. (37) (i.e., as the sum of a set of main error terms $\mathbf{T}_i$ - see the related discussion in Section 2), is compared with that directly obtained from NavLab error computations under free-inertial mode. If the curves are compared with the $\lambda/16$ threshold shown in Table 4 and imposed for guaranteeing SAS image quality, the constraint is not satisfied even in the LF application, given the SASIT length requested (see Fig. 4 in which the plots shown in Fig. 3 are zoomed on short SASIT length).

Although Eq. (37) is approximated, the curves compared in Fig. 3 fit well. This implies that the following analysis, performed on the single $\mathbf{T}_i$ error contributions,is consistent. The standard deviations of the error contributions $\mathbf{T}_0$, $\mathbf{T}_{1,a}$, $\mathbf{T}_{1,\omega}$, $\mathbf{T}_{3,a}$ and $\mathbf{T}_{3,\omega}$ are computed and shown separately in Fig. 5.

The discussion is focused on the terms depending on IMU sensor measurement errors, i.e, $\mathbf{T}_{1,a}$, $\mathbf{T}_{1,\omega}$, $\mathbf{T}_{3,a}$ and $\mathbf{T}_{3,\omega}$. As anticipated in Section 2, among these contributions the most significant effect to position displacement error comes from $\mathbf{T}_{1,a}$, which in turns depend on the accelerometer bias. This component is large and the fact that it varies in time with t^2 makes the error increase quickly. Among gyro errors

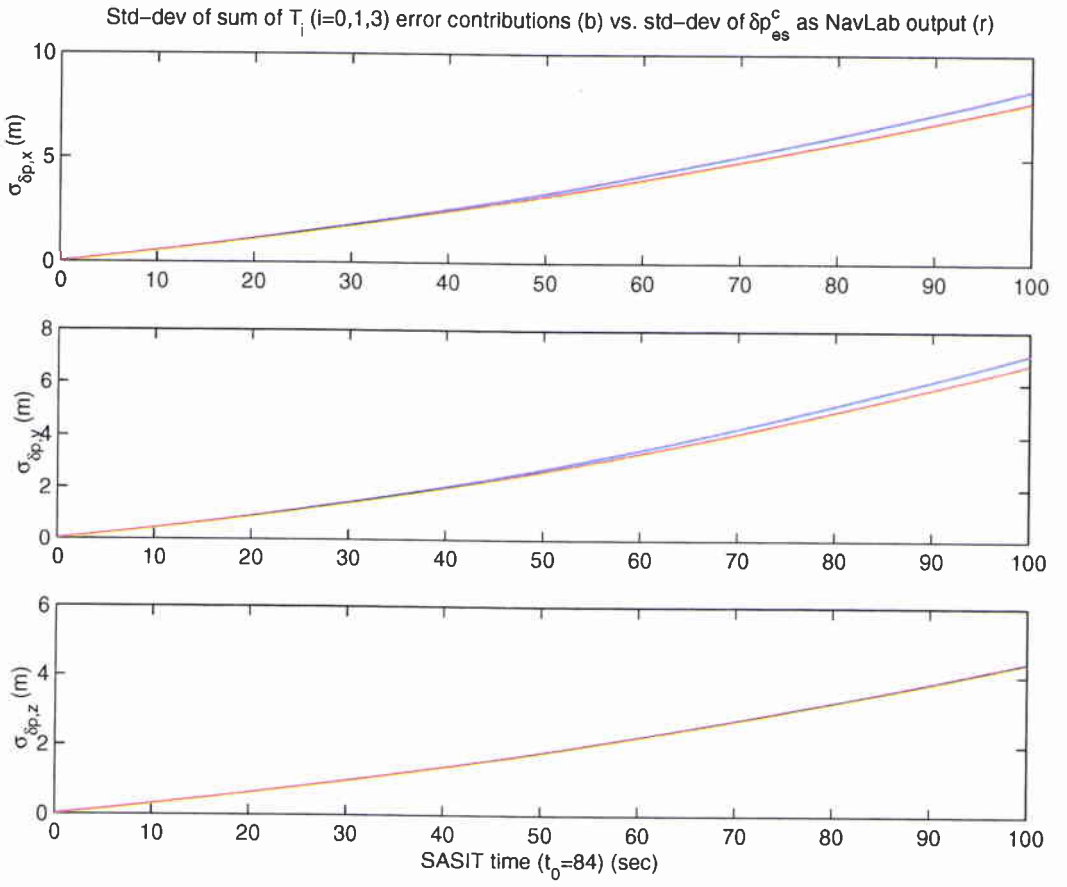

Figure 3 *Statistical analysis of the global position displacement error along a 100* s *aperture: standard deviation of the sum of* $\mathbf{T}_i$ *components computed over 150 runs vs. standard deviation of the position displacement error as derived from NavLab outputs.*

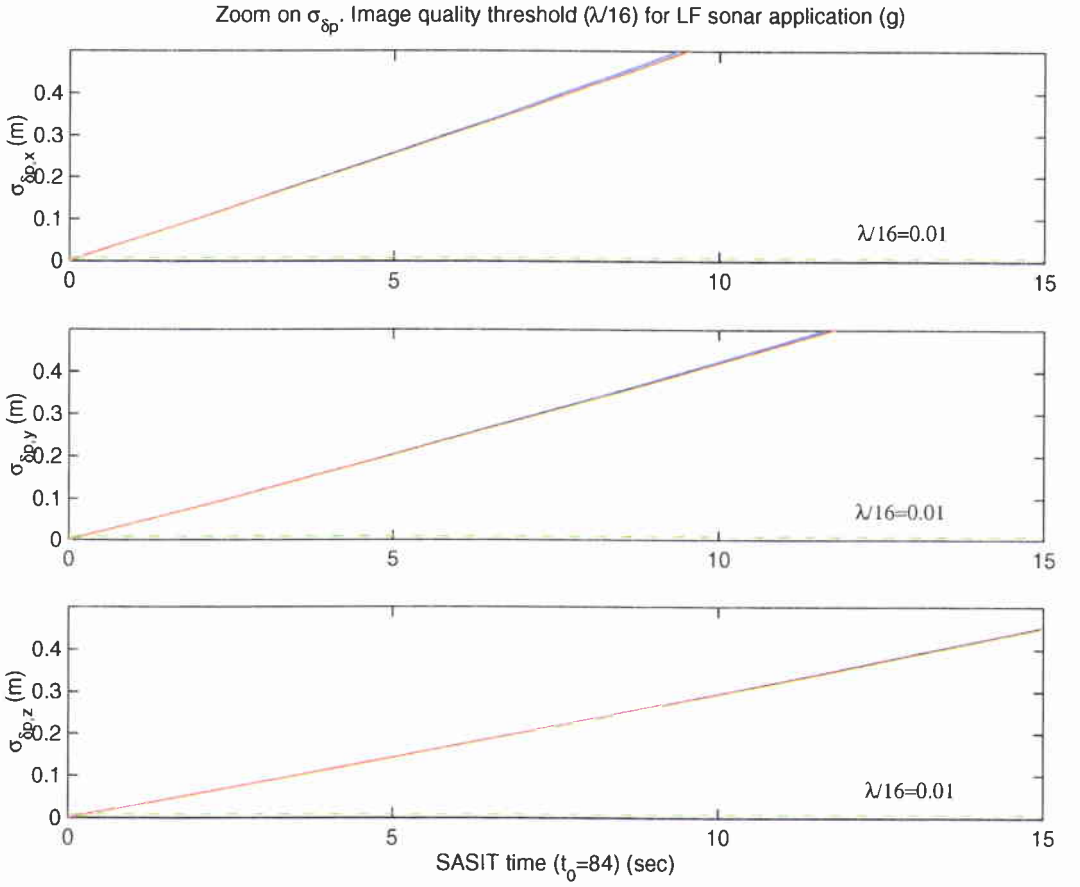

Figure 4 *Zoom of Fig. 3 on short SASIT length. Comparison of the standard deviation of global position displacement error to the image-quality threshold computed for a LF sonar application.*

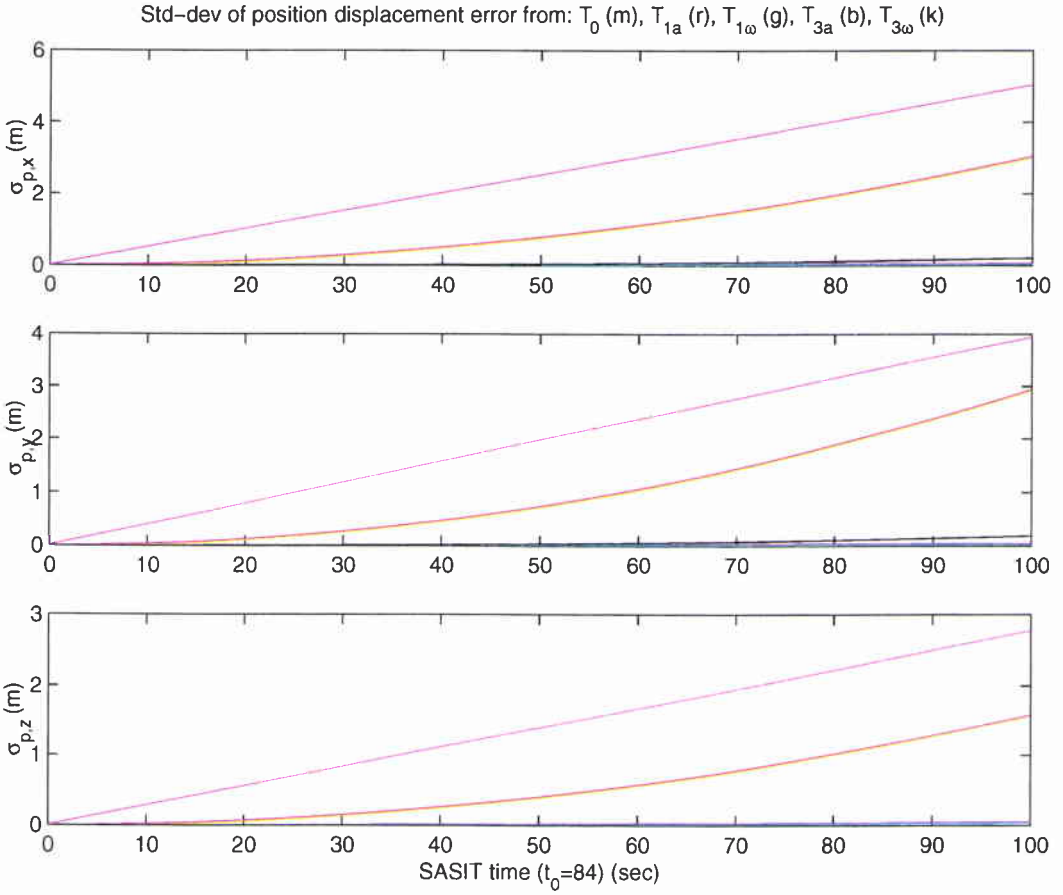

Figure 5 *Statistical analysis performed over 150 runs along a 100* s *aperture of the main position displacement error components.*

the main contribution is given by the gyro white noise, while the least significant contribution among the four considered comes from the gyro bias: the component standard deviations increases in time with t^3 but the gyro bias nominal value (from the selected sensor specifications) is so low that the error contribution remains low even after 100 s.

The lowest error contributions can be better appreciated by zooming on Fig. 5 as shown in Fig. 6 where only the terms $\mathbf{T}_{1,a}$, $\mathbf{T}_{1,\omega}$, $\mathbf{T}_{3,a}$ and $\mathbf{T}_{3,\omega}$ are plotted. It is possible to notice that the accelerometer bias contribution make the error to overcome both the LF and HF thresholds immediately after the aperture beginning even using the selected high-quality inertial sensor. This proves the unfeasibility of purely free inertial navigation for SAS applications and implies the necessity of designing a refined estimation architecture in which this error component in particular could be significantly reduced by integration with sensors of different nature.

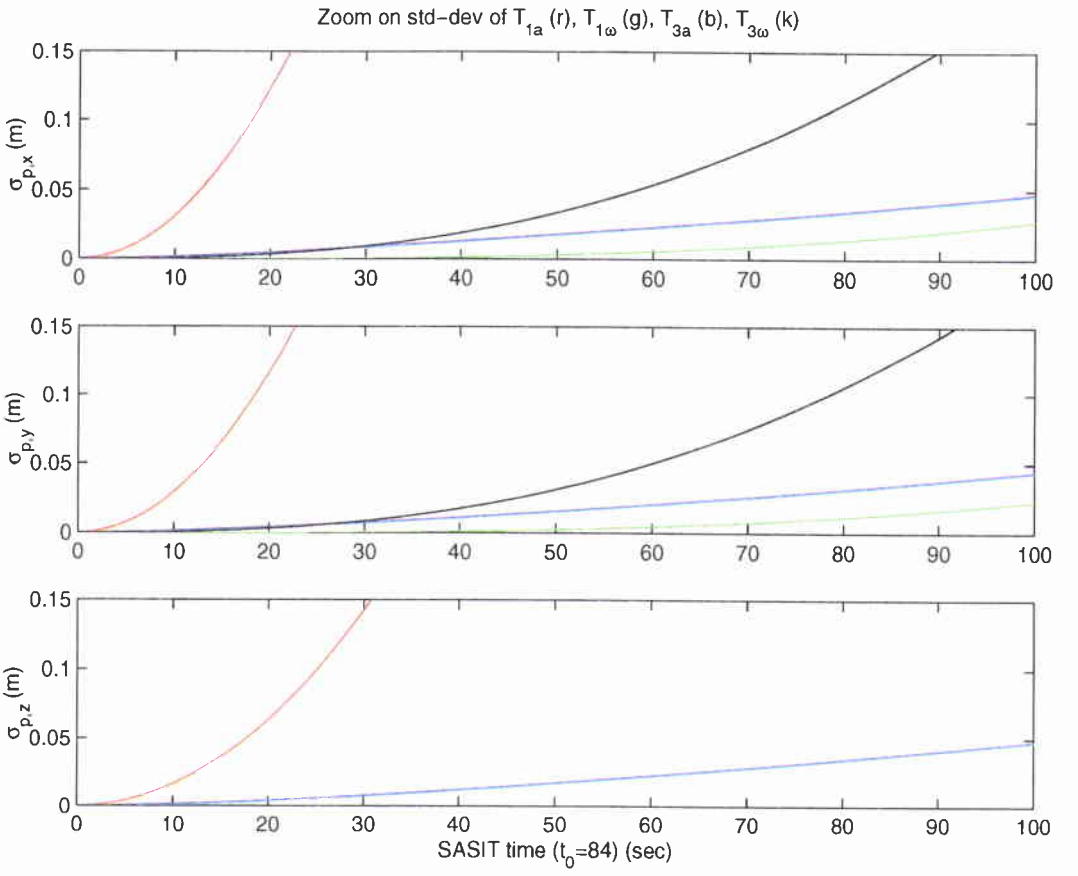

Figure 6 *Zoom of Fig. 5 on the lowest contributions of position displacement error.*

If a much shorter aperture (e.g., of 15 s is considered, which is in accordance with the parameters selected from typical applications (see Table 4), the time dependence of the four $\mathbf{T}$ components and consequently the unfeasibility of free-inertial navigation are even better outlined (see Fig. 7).

The standard deviations of the four error contributions $\mathbf{T}_{1,a}$, $\mathbf{T}_{1,\omega}$, $\mathbf{T}_{3,a}$ and $\mathbf{T}_{3,\omega}$, computed from 150 simulation runs are now compared to their approximated analytical formulas in Eqs (42) and (43) in order to validate the consistency of the approximations. The comparison results are presented in Figs 8, 9, 10 and 11 respectively. Despite the relatively low number of runs over which to make the statistical analysis, the plots generally confirm the validity of the formulas, which, as outlined in Section 2, are very useful to separate the various error contributions coming from the IMU sensor measurement errors, hence to interpret the error results in terms of these components. The number of runs for statistical convergence is particularly critical in the statistical analysis of the error contributions $\mathbf{T}_{3,a}$ and $\mathbf{T}_{3,\omega}$, depending on the accelerometer and gyro white noise respectively. In these two cases the theo-

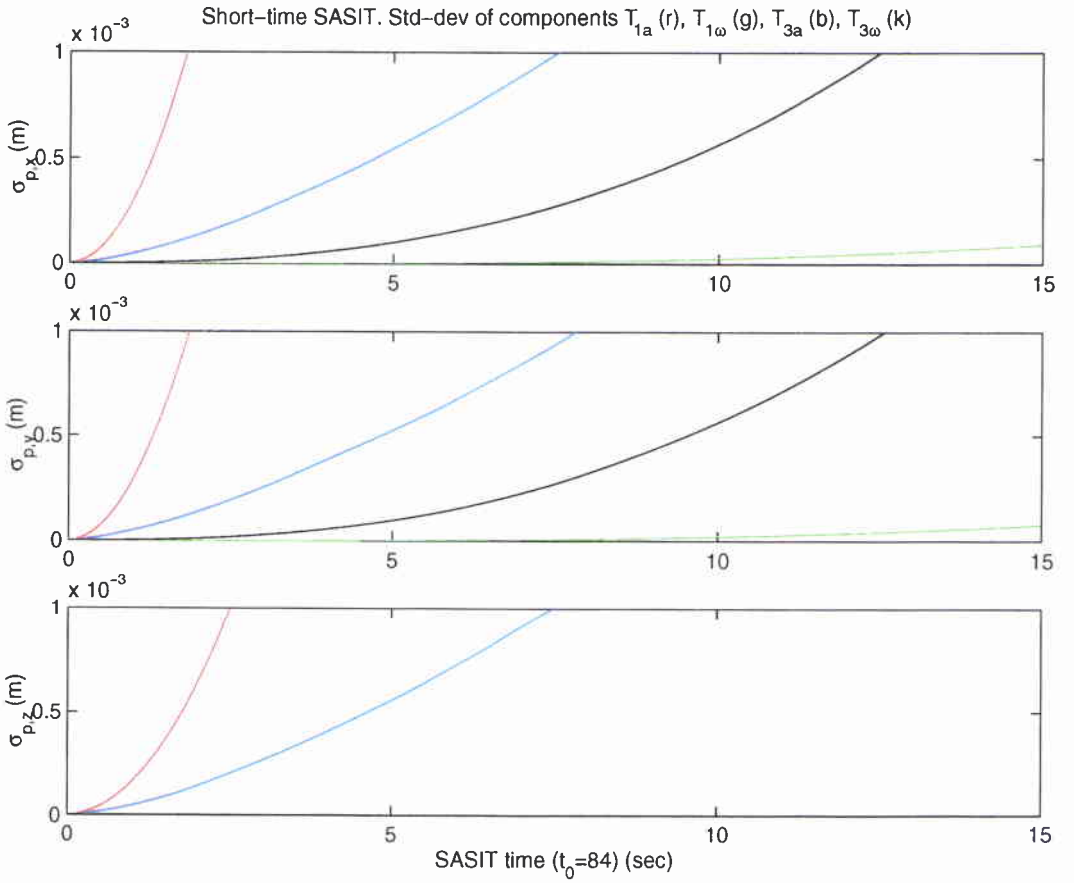

Figure 7 *Short-term (15 s) aperture: main contributions of position displacement error.*

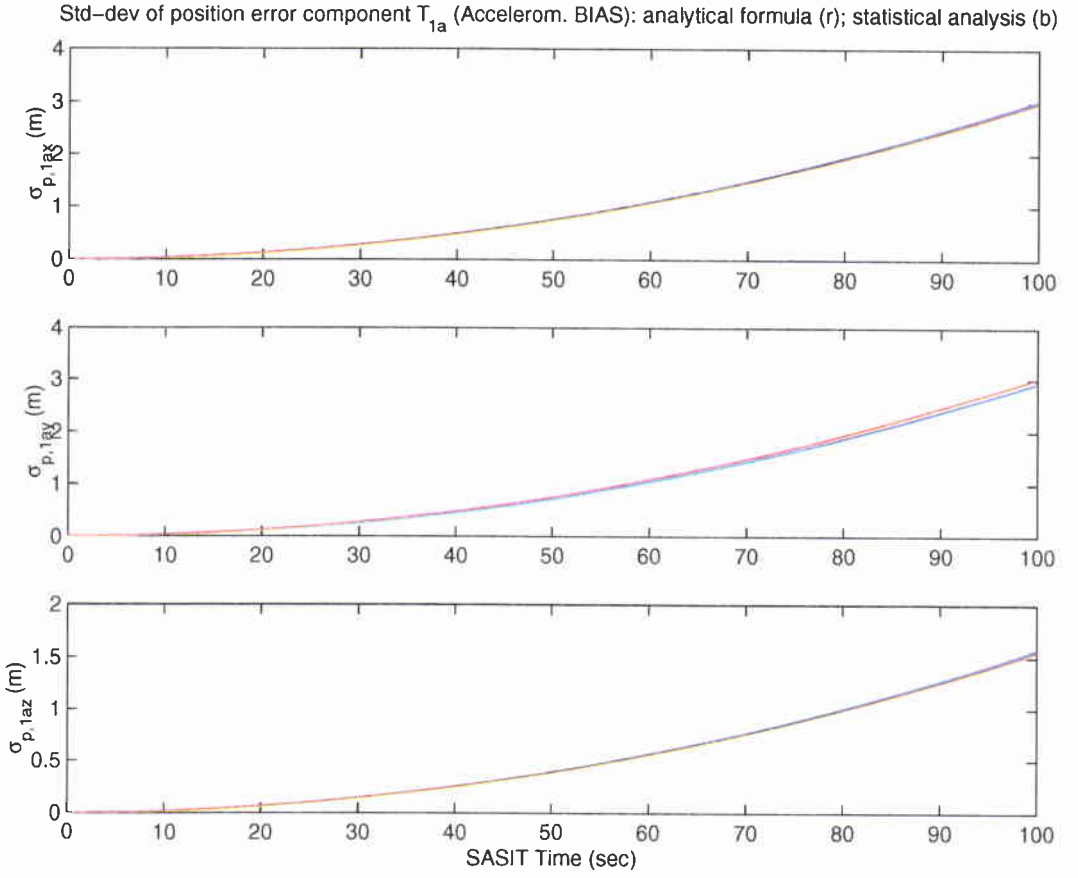

Figure 8 *Comparison between the approximated analytical formula (Eq. (42)) of the* $\mathbf{T}_{1,a}$ *std-dev and the statistical analysis result obtained over 150 simulation runs (Fig. 5).*

retical formulas for the standard deviation (Eq. (43)) are rigorous, but the statistical computation from NavLab simulation results would have needed a larger number of runs (i.e., much larger than the selected 150) in order to be consistent, hence to converge to the theoretical curve. The deviation of the statistical computations with respect to the analytical formulas is particularly evident on a relatively long period (of the order of 100 s), as shown from the comparison of Figs 10 and 11 with Figs 12 and 13, where a shorter aperture (of 15 s) is selected. This effect is due to the high order dependence of the two standard deviations on time, particularly in the case of gyro random noise contribution.

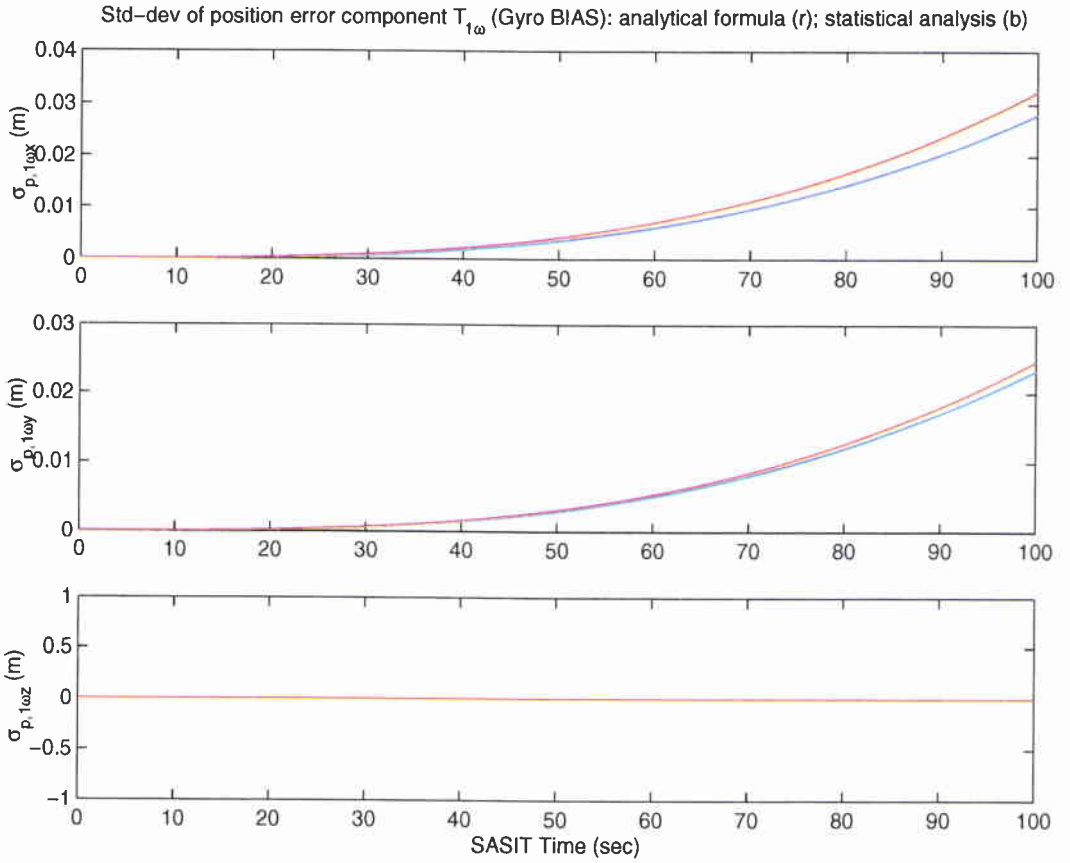

Figure 9 *Comparison between the approximated analytical formula (Eq. (42)) of the* $\mathbf{T}_{1,\omega}$ *std-dev and the statistical analysis result obtained over 150 simulation runs (Fig. 5).*

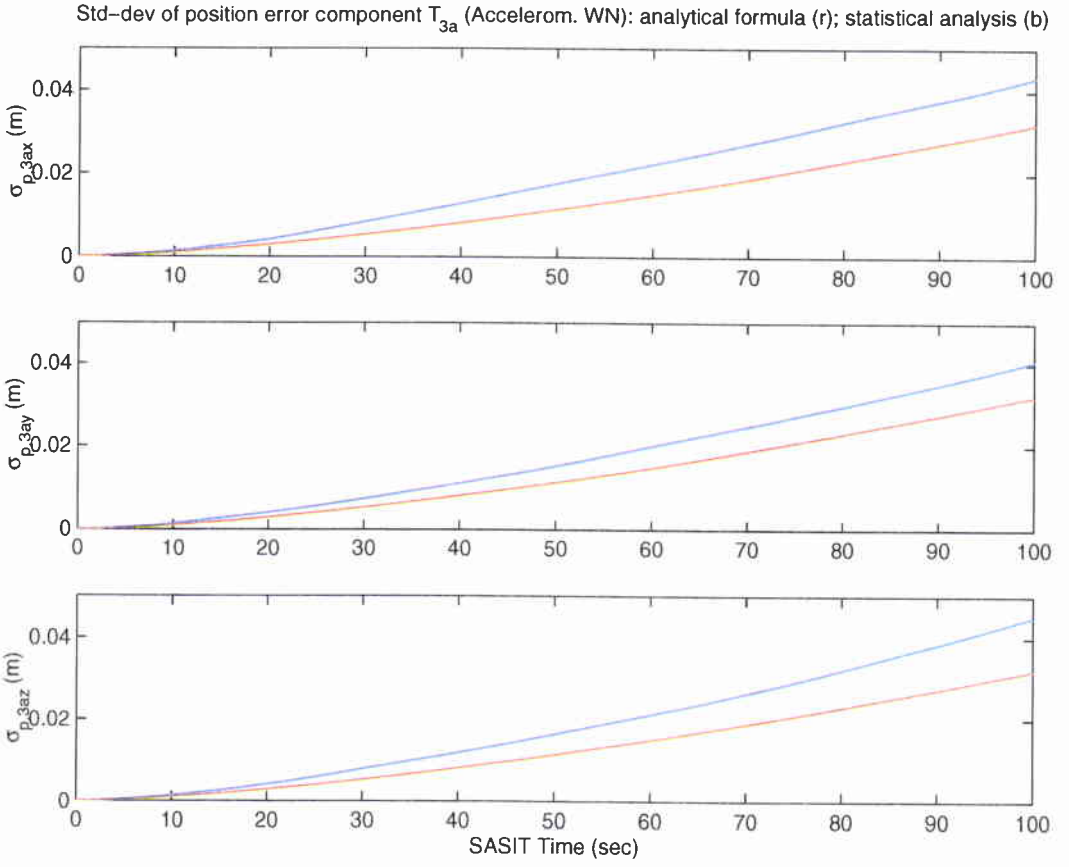

Figure 10 *Comparison between the analytical formula (Eq. (43)) of the* $\mathbf{T}_{3,a}$ *std-dev and the statistical analysis result obtained over 150 simulation runs (Fig. 5).*

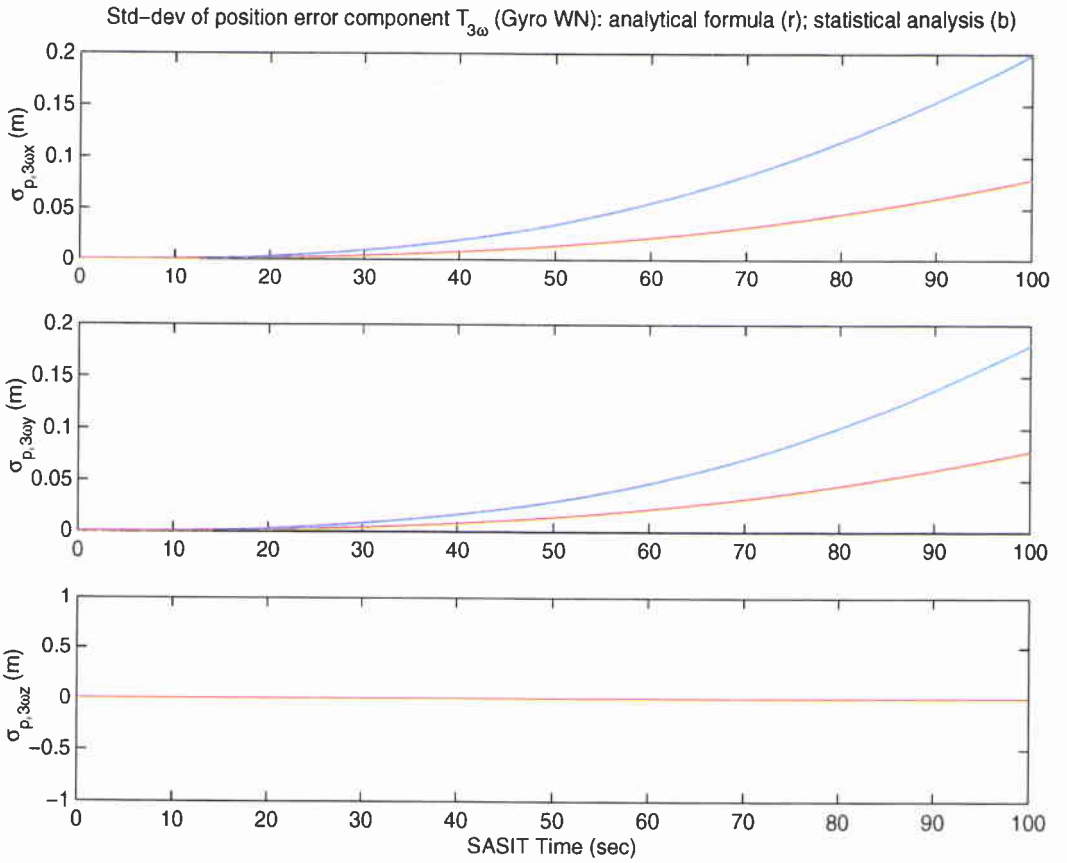

Figure 11 *Comparison between the analytical formula (Eq. (43)) of the* $\mathbf{T}_{3,\omega}$ *std-dev and the statistical analysis result obtained over 150 runs (Fig. 5).*

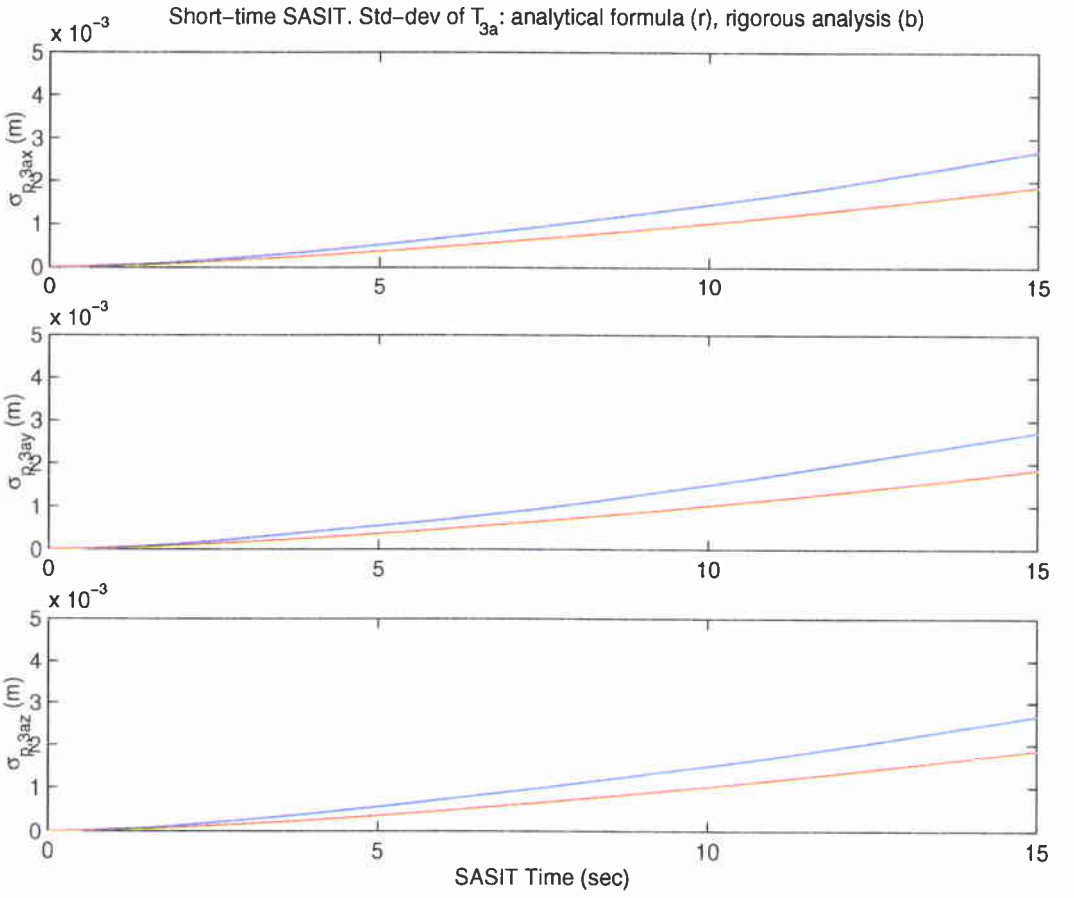

Figure 12 *Short-time SASIT. Comparison between the theoretical formula (Eq. (43)) of the* $\mathbf{T}_{3,a}$ *std-dev and the statistical analysis computed over 150 runs.*

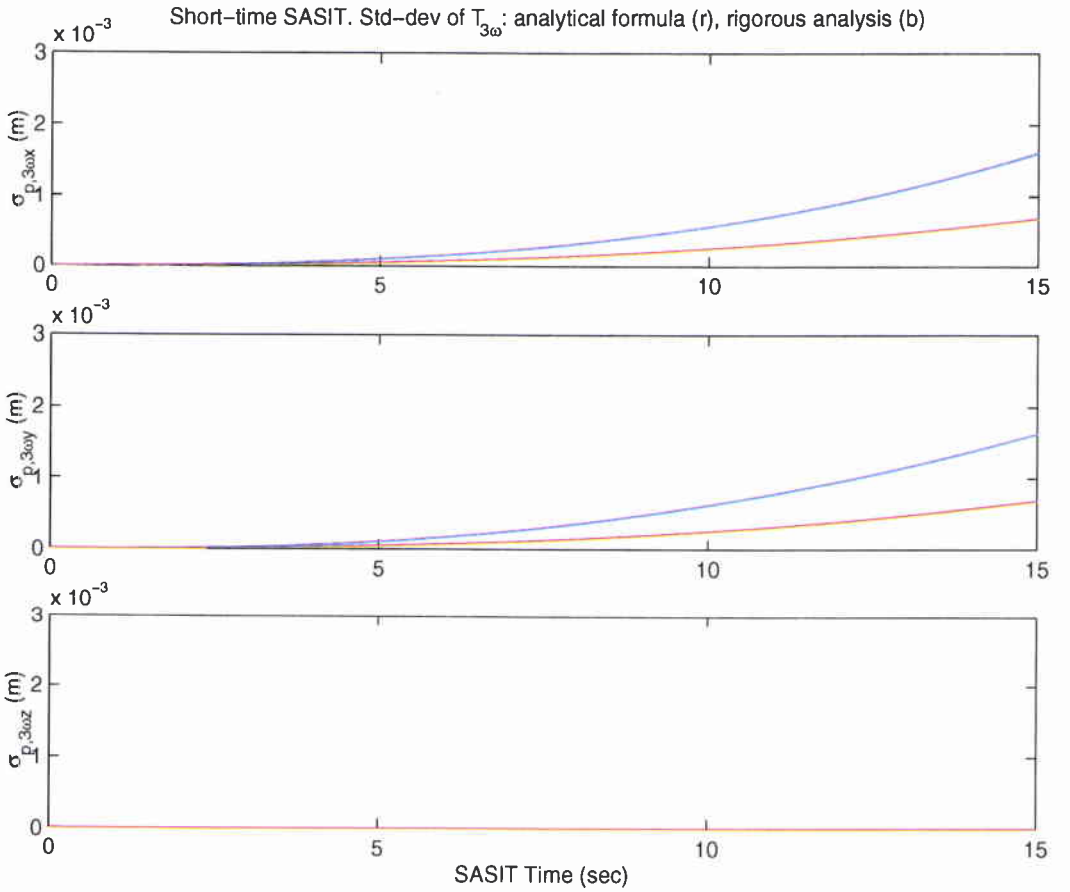

Figure 13 *Comparison between the theoretical formula (Eq. (43)) of the* $\mathbf{T}_{3,\omega}$ *std-dev and the statistical analysis result obtained over 150 runs.*

3.3.2 Simulated attitude errors

The statistical analysis of the error in attitude displacement along a SAS aperture with respect to the SAS starting point is also performed under free-inertial navigation conditions based on 150 Navlab runs under the test configuration specified in Section 3.2.

The analysis of the global error in attitude displacement is considered first. In Fig. 14 the standard deviation computed on 150 runs of the attitude misalignment as expressed in Eq. (37) (i.e., as the sum of a set of main error terms P_i - see the related discussion in Section 2), is compared with that directly obtained from NavLab error computations under free-inertial mode. If the error values on the plots are compared with the values of the threshold $\lambda 8 L_a$) proposed in Table 4 for guaranteeing SAS image quality in either LF, HF and survey cases, it is clear that the computed error remains much lower even over SASIT lengthswhich are much longer than the selected ones. This is caused by the very high quality of the selected IMU gyro.

Although Eq. (37) is approximated, the curves compared in Fig. 14 fit well. This implies that the analysis, performed on the single $\mathbf{P}_i$ error contributions,is consistent. The error components $\mathbf{P}_{1,\omega}$ and $\mathbf{P}_{3,\omega}$ are statistically evaluated by means of the computation of their standard deviations as time varies and plotted separately in Fig. 15. It is immediately clear that for the selected IMU sensor, the attitude error contribution due to the gyro white noise is more significant than that due to gyro bias. Further, the dependence of random walk error standard deviation with the square root of time is evident.

The standard deviation computations based on statistical analysis of NavLab simulations are compared with the approximated analytical formulas provided in Section 2.2.4. Figures 16 and 17 show the comparison results. It is evident that the curve fitting is good, hence the corresponding analytical formulas are shown to be accurate, even over a long-term aperture of 100 s. This is particularly evident for the error component due to gyro white noise (Fig. 17). Here the limited number of runs seems not to affect the accuracy of standard deviation estimation (as noticed in the cases of $\mathbf{T}_{3,a}$ and $\mathbf{T}_{3,\omega}$ because the time dependence is of orders equal to (accelerometer error contribution) or less than (gyro error contribution) the first.

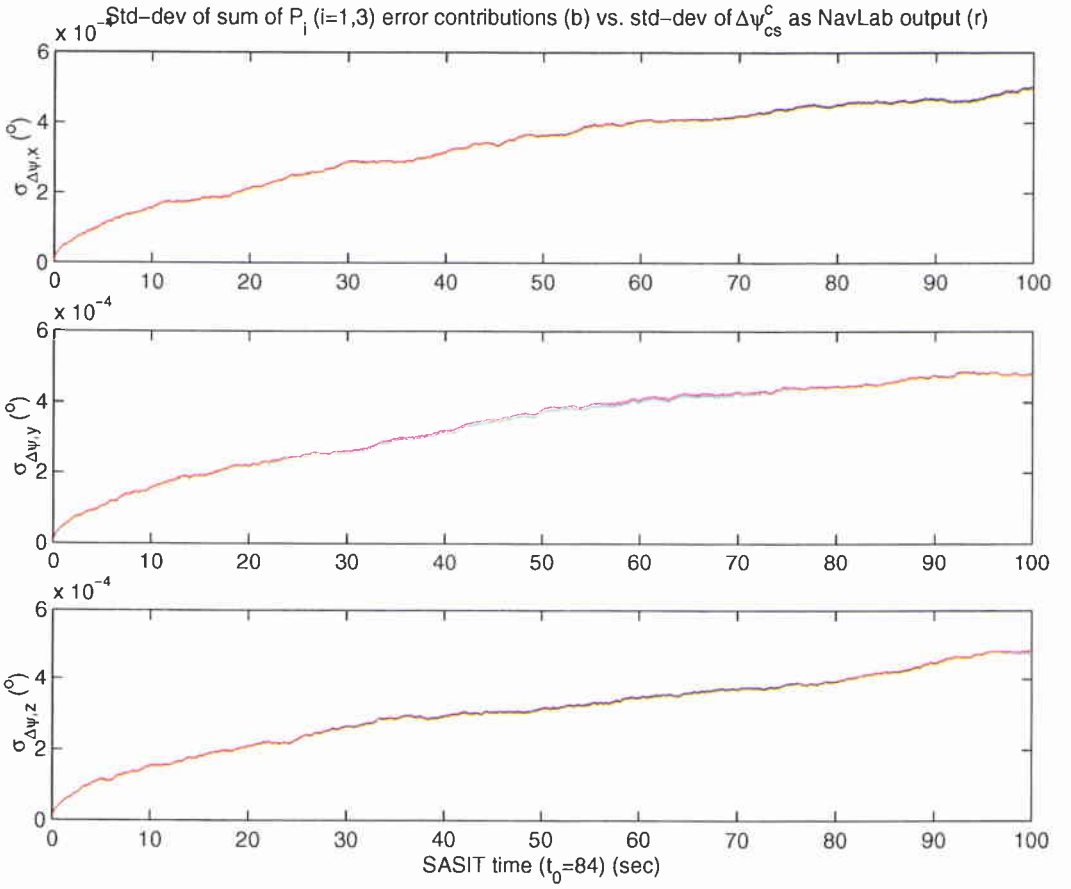

Figure 14 *Statistical analysis of the global attitude displacement error along a 100 s aperture: standard deviation of the sum of* $\mathbf{P}_i$ *components computed over 150 runs vs. standard deviation of the error as derived from NavLab outputs.*

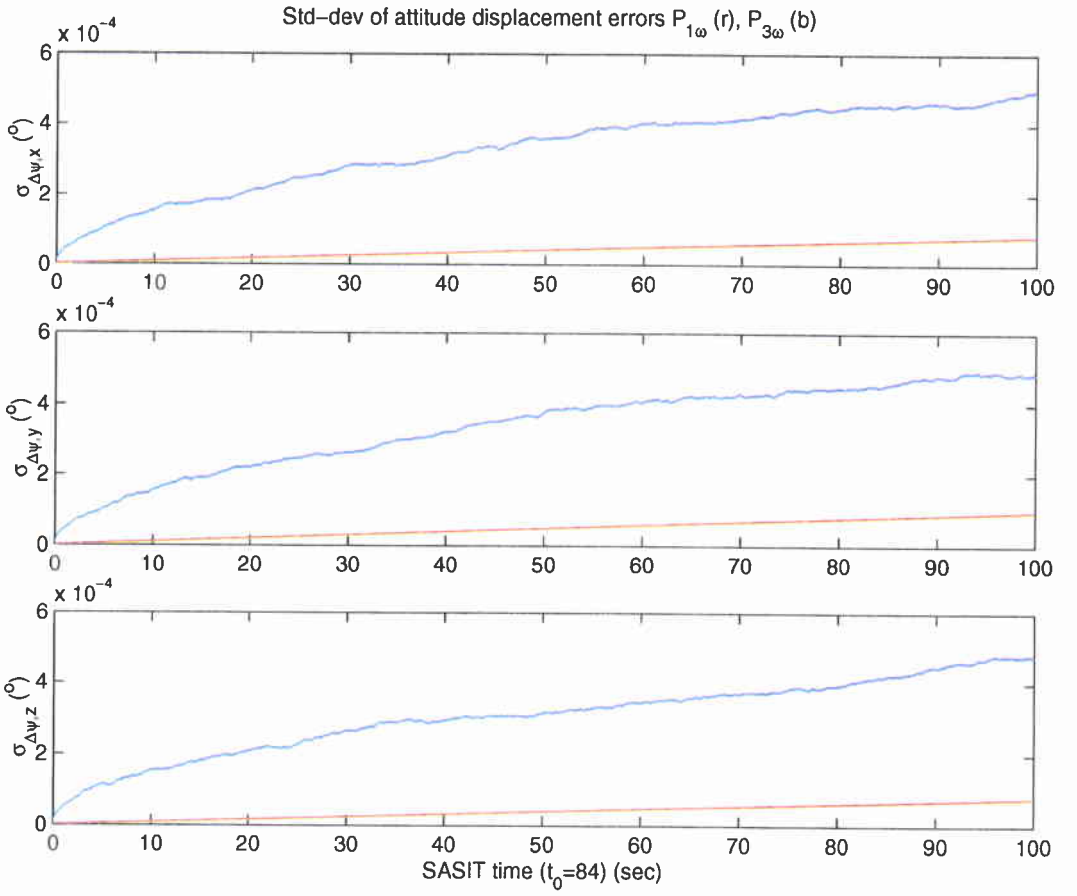

Figure 15 *Statistical analysis performed over 150 runs along a 100* s *aperture of the main attitude displacement error components.*

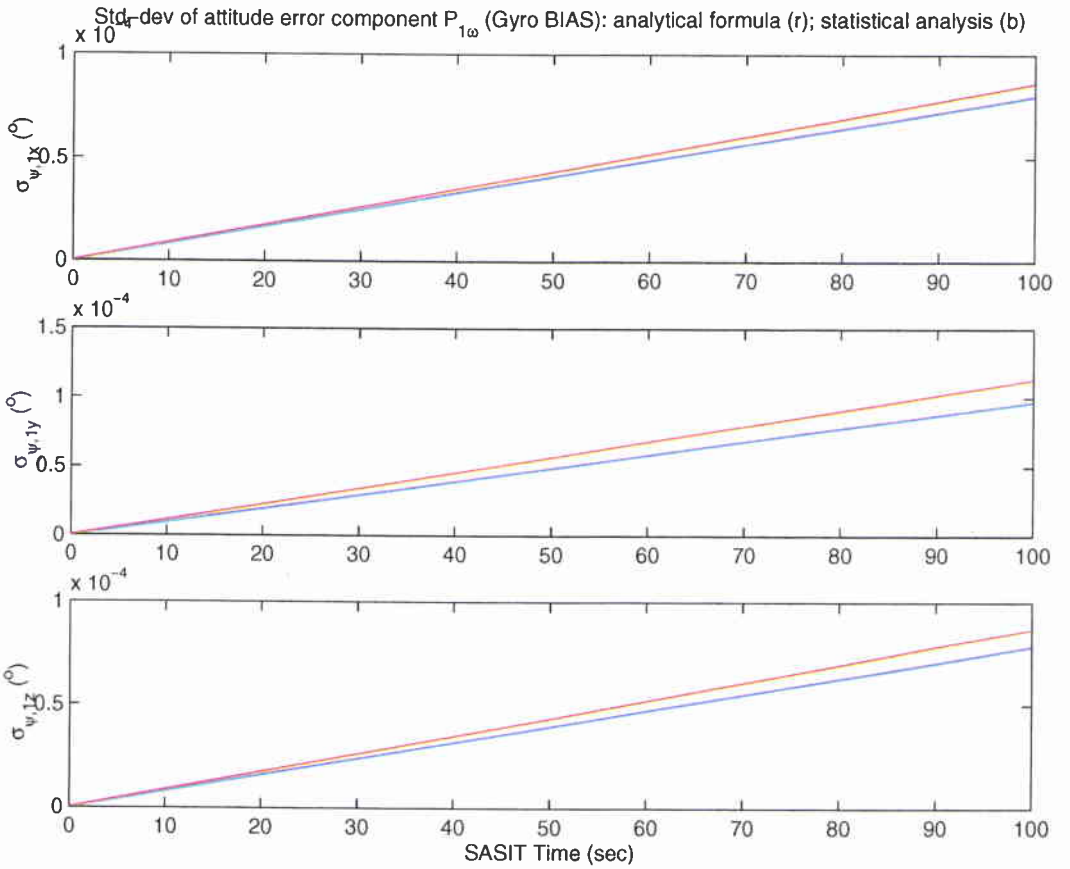

Figure 16 *Comparison between the approximated analytical formula (Eq. (46)) of the* $\mathbf{P}_{1,\omega}$ *std-dev and the statistical analysis result obtained over 150 simulation runs (Fig. 15).*

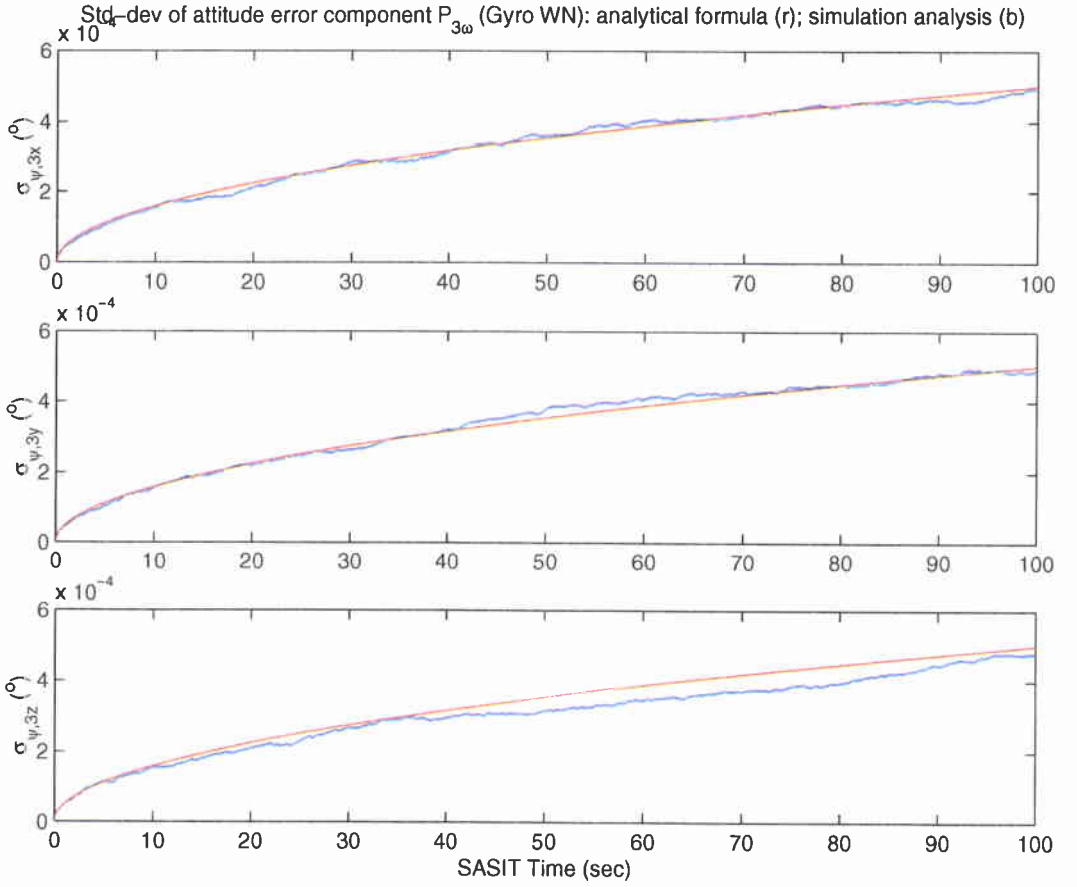

Figure 17 *Comparison between the analytical formula (Eq. (47)) of the* $\mathbf{P}_{3,\omega}$ *std-dev and the statistical analysis result obtained over 150 runs (Fig. 15).*

4

Conclusions

The feasibility of using a high quality INS in free-inertial mode for achieving short-term positioning and attitude accuracy compatible with the requirements imposed by SAS processing has been studied.

The theoretical investigation based on ψ-angle error analysis of the navigation equations has been validated by simulation. The statistical analysis has been performed on a SAS integration time of up to 100 s.

IMU sensor measurement errors, as specified by the constructor, were taken into account separately and their effects on the sonar position and orientation global error evaluated and interpreted. The analysis is useful for selecting the most suitable IMU to achieve the specified SAS accuracy requirements, and for focusing future activities on the optimization of a multi-sensor navigation system able to maintain low the error components which influence the positioning performance in SAS applications. The global navigation architecture will integrate the IMU measurement with either traditional aiding navigation sensors (DGPS, Doppler Velocity Log, Depthmeter, etc.), as in standard Aided Inertial Navigation Systems (AINS) [7][4], or sonar-based micronavigation estimates (e.g., achieved by DPCA technique [2][3]).

One of the main results achieved through the free-inertial error analysis was the identification of the *accelerometer bias* as one of the most critical IMU error components for short-term position accuracy, as it gives rise to big quadratic position drift. Bias will be significantly reduced by integration with SAS-based micronavigation techniques. High accuracy attitude estimation (re. the constraints imposed by typical SAS applications) has been achieved even in free inertial mode, which shows the feasibility of using a high quality IMU for this particular purpose. High-accuracy attitude estimation is of great importance for achieving high SAS image quality.

Future work will include:

- Optimization and performance evaluation of a standard AINS system (consisting of INS, DVL, depthmeter, etc.) able to improve the free-inertial short-term navigation results discussed in this work (with the help of an adapted NavLab version).
- Design of a new navigation architecture (consisting of the AINS system in-

tegrated with SAS micronavigation) to improve both long- and short-term navigation accuracy (this will imply the integration of DPCA into a new SAS-extended NavLab tool).

- Evaluation of the accuracy performances of the new navigation architecture in terms of SAS image quality by simulation (by means of the SAS-extended NavLab tool) and using experimental data.

5 Acknowledgements

The authors wish to thank the Norwegian Defence Research Establishment (NDRE), and in particular Nils Storkersen, Bjorn Jalving and Kenneth Gade for the delivery of NavLab and their much appreciated cooperation. Many thanks to P. Guerrini for his significant contribution in the definition of characteristics and in the selection of the AINS system.

References

[1] "Synthetic Aperture Sonar motion compensation system. Analysis and simulation study," Tech. Rep. 40910020-R0, Applanix (Applied Analytics Corporation) and TSS, March 1997.

[2] M. Pinto, S. Fioravanti, and E. Bovio, "Accuracy of synthetic aperture sonar micronavigation using a displaced phase centre antenna," SM-352, NATO SACLANT Undersea Research Centre, La Spezia, Italy, Feb. 1999.

[3] A. Bellettini, M. Pinto, and S. Fioravanti, "Preliminary experimental investigation of synthetic aperture sonar micronavigation," SM-355, NATO SACLANT Undersea Research Centre, La Spezia, Italy, 1999.

[4] K. Gade, "Intergrering av treghetsnavigasjon i en autonom undervannsfarkost," FFI/Rapport-97/03179, Forsvarets ForskningsInstitutt (FFI), Kjeller, Norway, July 1997.

[5] D. O. Benson, "A comparison of two approaches to pure-inertial and Doppler-inertial error analysis," *IEEE Trans. on AES*, vol. AES-11, pp. 447–455, July 1975.

[6] R. G. Brown and P. Y. C. Hwang, *Introduction to random signals and applied Kalman filtering.* New York: J. Wiley Sons, Inc., second ed., 1985.

[7] D. H. Titterton and J. L. Weston, *Strapdown inertial navigation technology.* United Kingdom: P. Peregrinus Ltd., first ed., 1997.

Annex A

Navigation reference frames and transformations between them

A.1 Main navigation frames

In order to develop a navigator for the INS and eventually to integrate data from inertial and non-inertial positioning/navigation sensors, it is necessary to define the appropriate sets of Cartesian coordinate reference frames. Each frame is an orthogonal, right-handed system of three axes. The fundamental frames involved in the solution of the navigation problem proposed in this report are defined in the following.

- **Earth frame** (e): has its origin O_e at the Earth's centre and its axes, namely X_e, Y_e and Z_e, fixed with respect to the Earth. X_e coincides with the Earth's polar axis (which is assumed to have invariant direction) oriented towards North, and the other two lay on the Equatorial plane with Y_e passing through the Greenwich meridian [7]. The frame rotates with the Earth at the Earth angular rate Ω around the X_e axis.

- **Inertial frame** (i): its axes X_i, Y_i and Z_i are fixed with respect to the fixed stars. For convenience its origin is chosen to coincide with the Earth centre and its X_i axis coincides with X_e [7].

- **Local frame** (l): is the local geographic frame centred on the average Earth surface at the latitude and longitude of the vehicle current location, i.e., of the vehicle reference point B in which the navigation system is assumed to be installed. Its axes X_l, Y_l and Z_l are aligned with the directions of true North, East and local vertical (Down) respectively [4]. Its turn rate with respect to the Earth, $\vec{\omega}_{el}$, is caused by the motion of B (i.e., of the vehicle and also of the sonar phase centre) with respect to the Earth and is also referred to as "transport rate".

- **Body frame** (b): its axes X_b, Y_b and Z_b are aligned respectively with the Roll, Pitch, Yaw axes of the platform (i.e., the "body") on which the navigation system is installed, and its origin is assumed to coincide with the INS reference point B.

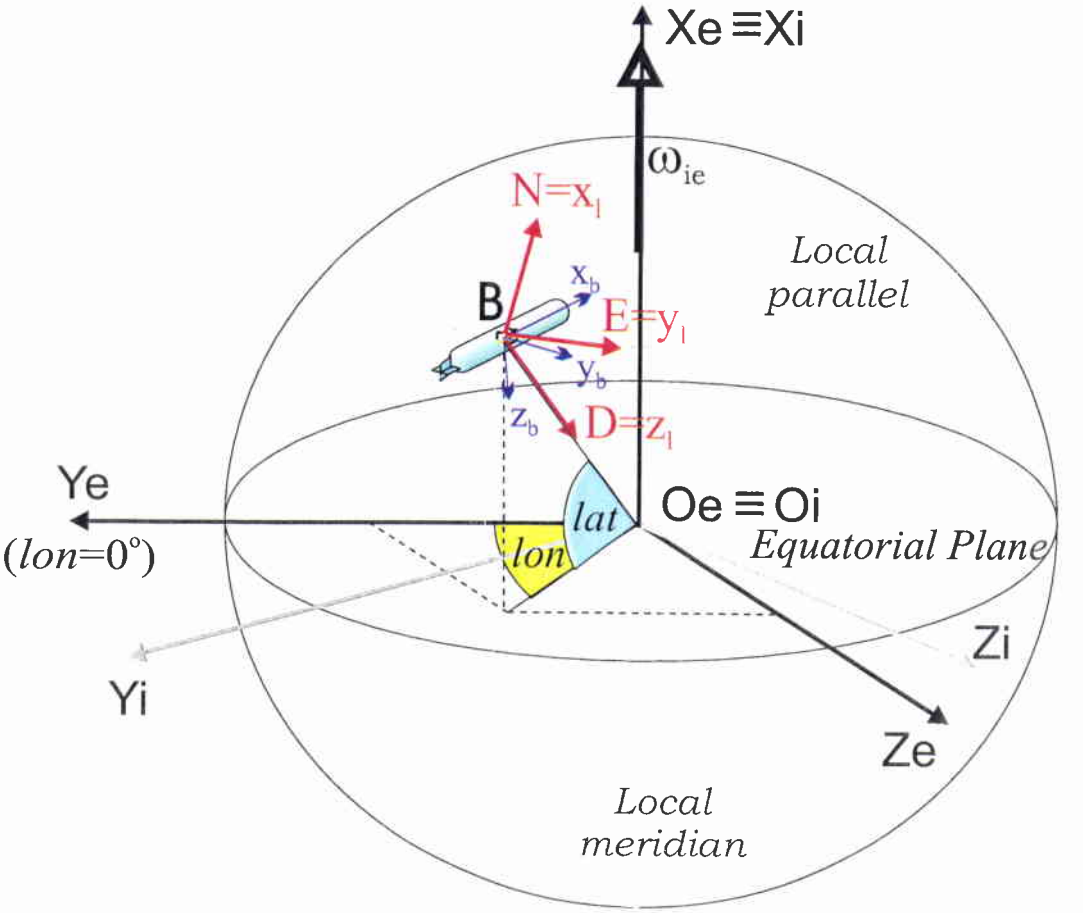

Figure 18 *Scheme of the Earth (e), Inertial (i), current Local-level (l) and Body (b) reference frames.*

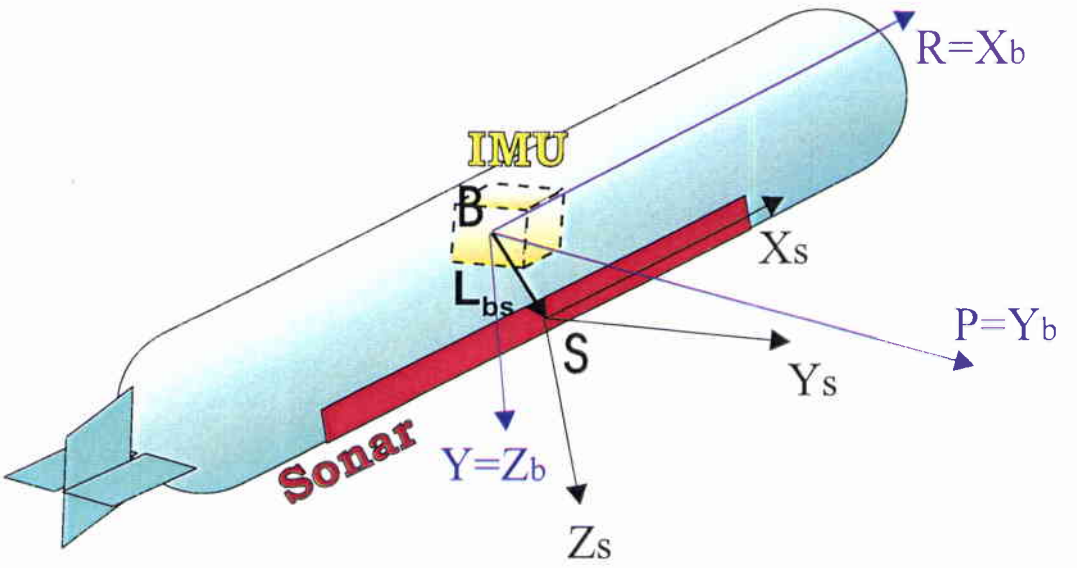

Figure 19 *Scheme of the Body (b) and Sonar (s) frames.*

Figure 18 shows the Earth-fixed, Inertial, Local level and Body frames for navigation over the Earth; Figure 19 focuses on the Body frame and another coordinate system, the Sonar frame, which is derived from the mentioned fundamental ones through translation/rotation and is useful for SAS evaluation:

- **Sonar frame** (s): is a "body frame" with origin in the sonar array phase centre S (i.e., translated of the lever arm $\mathbf{L}_{bs}$ from the body frame origin B) and roll set to zero (i.e., its y axis is always on the horizontal plane).

Another frame involved in the error analysis is the:

- **"initial" local level frame** (l_0): is the local frame fixed in the position occupied by the navigation system at the aperture starting time t_0.

The comparison between the initial and current local level frames and their relation with the body frame are outlined in Fig. 20. The rotation between the initial and current local frames is exaggerated. The relation between the body and sonar frames is shown in vertical projection in Fig. 21.

It is necessary to define how to transform any 3-D dynamic quantity, represented by the generic three-element vector $\mathbf{k}$, originally expressed in a reference frame m, into another reference frame n. This transformation is carried out through the so-called Direction Cosine Matrix (DCM) from m to n, C_m^n (3×3), by means of the equation:

$$\mathbf{k}^n = C_m^n \mathbf{k}^m. \tag{A1}$$

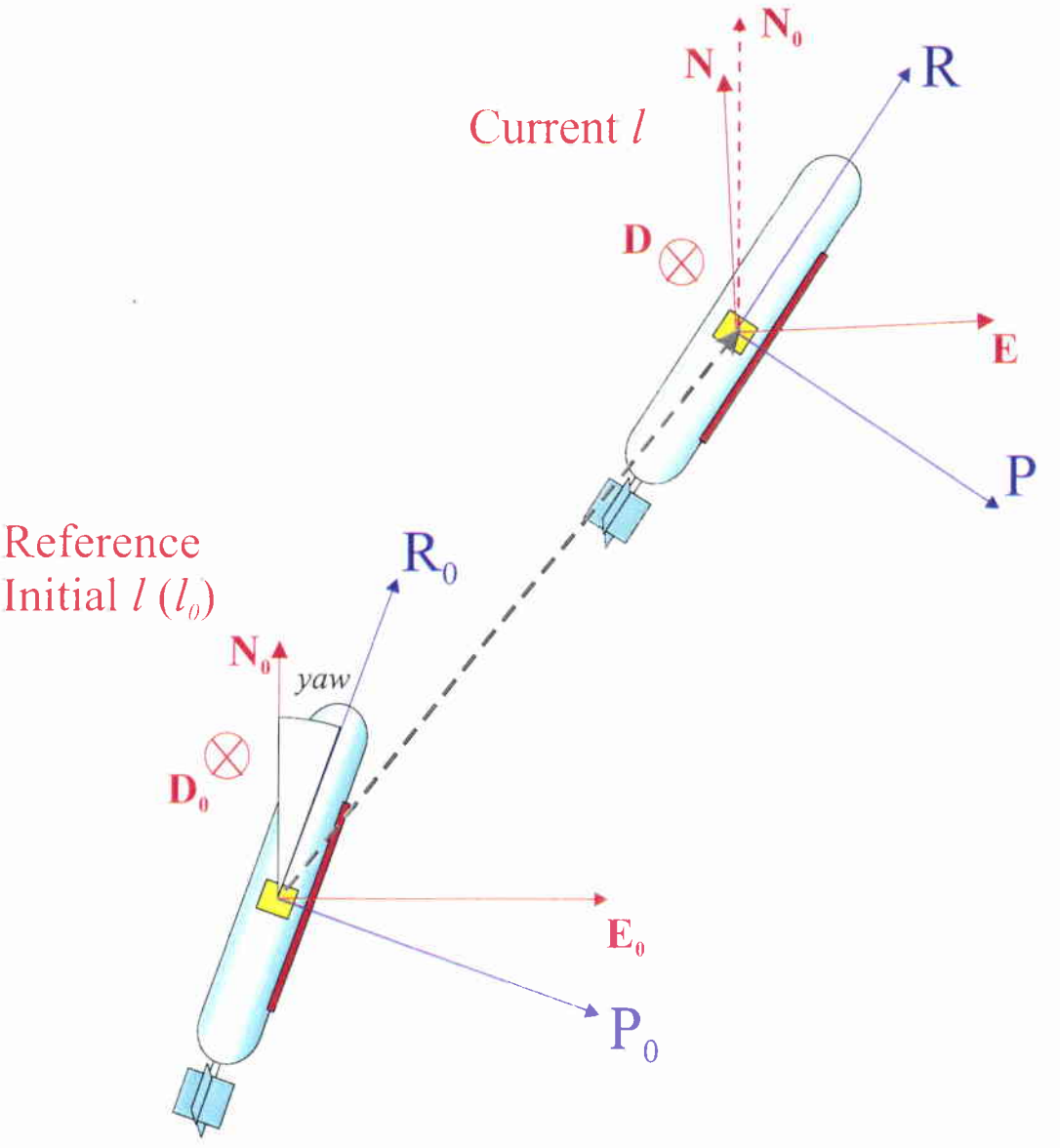

Figure 20 *Schematic of the relation between the body and local level frames between the initial time t_0 and the current time t within a SASIT (horizontal projection of the vehicle trajectory).*

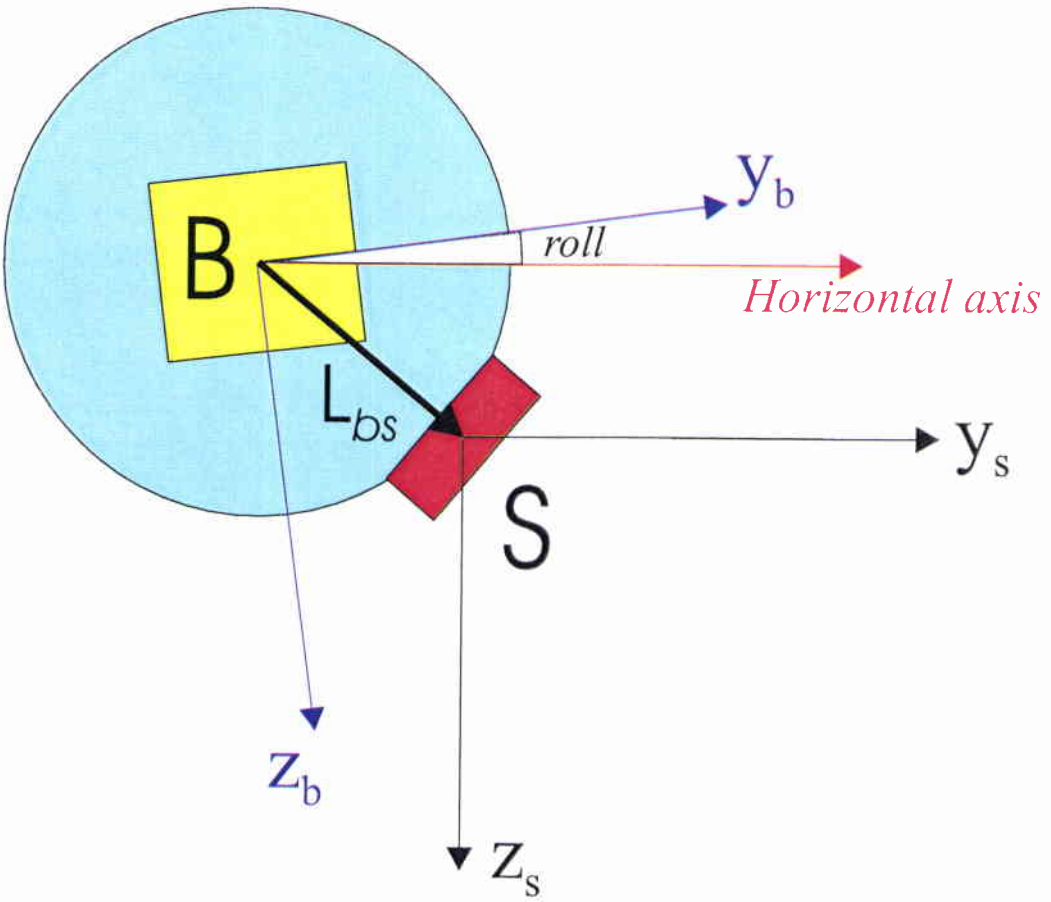

Figure 21 *Schematic of the relation between the body and sonar reference systems (projection on the body cross-section plane).*

The DCM dynamics follow the law:

$$\dot{C}_m^n = C_m^n(\omega_{nm}^m \wedge) = C_m^n \mathbf{\Omega}_{nm}^m, \tag{A2}$$

where $\omega_{nm}^m = [\omega_{nm,x}^m, \omega_{nm,y}^m, \omega_{nm,z}^m]^T$ is the turn rate of the m frame with respect to the n frame decomposed in the m frame, and the $[3 \times 3]$ matrix $\mathbf{\Omega}_{nm}^m$, defined as:

$$\mathbf{\Omega}_{nm}^m = \begin{bmatrix} 0 & -\omega_{nm,z}^m & \omega_{nm,y}^m \\ \omega_{nm,z}^m & 0 & -\omega_{nm,x}^m \\ -\omega_{nm,y}^m & \omega_{nm,x}^m & 0 \end{bmatrix}, \tag{A3}$$

represents the skew symmetric form of ω_{nm}^m.

A.2 Relationship between "computed" and "ideal" reference frames

As anticipated in the previous subsection, the "ideal" reference frame selected as navigation system for short-term (over a SASIT period) error analysis is the initial local level frame l_0, i.e., a fixed local level frame centred on the Earth surface at the latitude and longitude of the body position at the aperture beginning (t_0). According to the ψ angle methodology, the navigation equations can be attempted to be solved by the navigation system in a frame which is only the "corrupted" version of the ideal one. This frame, called *computer* frame c, is defined as the reference frame in which the navigation equations are solved by the computer. In this case c is the computed version of l_0.

The two frames are assumed to be generally misaligned, i.e., to differ for an angular rotation ψ_{l_0c}. This vector is called angular misalignment of c with respect to the ideal l_0 frame and is assumed to be small. As the error analysis is performed on the position error of the body, in order to formalize and solve the navigation error equations it is necessary to define also the misalignment between the body and computer frames, namely ψ_{cb}. This can be defined in terms of ψ_{l_0c} and of the misalignment between the body and local level frames, ψ_{l_0b}, as follows:

$$\psi_{cb} = \psi_{l_0b} - \psi_{l_0c}. \tag{A4}$$

The relation between the b, l_0 and c coordinate frames is shown in Fig. 22, where, for the sake of simplicity, misalignment is limited to the xy plane (i.e., to the $\psi(z)$ components of the angular misalignment vectors).

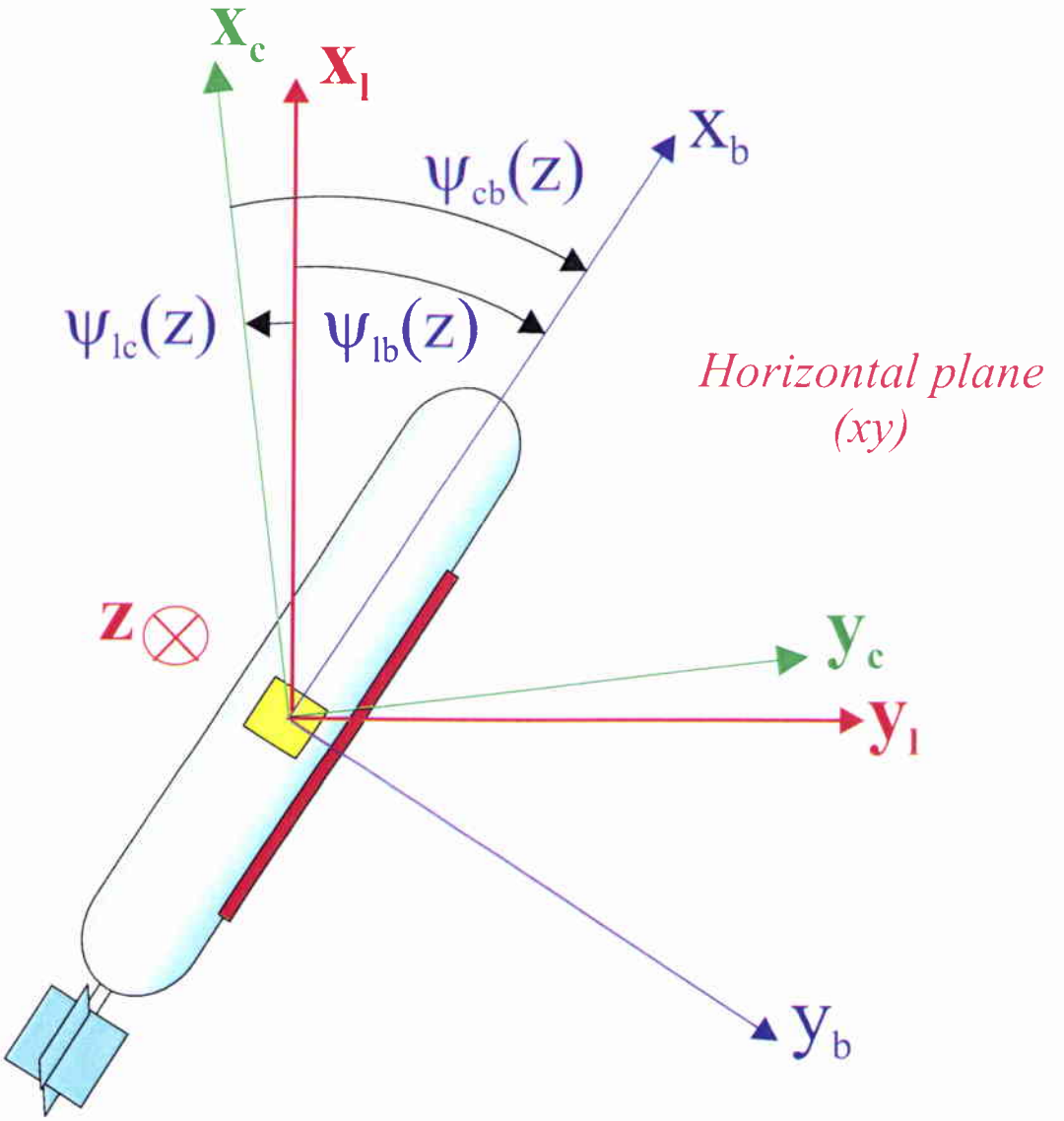

Figure 22 *Simplified scheme of the relation between the "ideal" Local level navigation frame l_0 (indicated here as l), its "computed" version c and the body frame b. In the example misalignment is limited to the z angle components.*

Annex B

Derivation of the errors in position and angle displacement in terms of vehicle dynamics and IMU sensor errors (Eq. 20)

From Eq. (19), which is the result of the ψ-angle short-term error analysis described in Section 2, the position and attitude displacement errors re. the aperture beginning can be derived as follows. It is assumed that the computer frame c is fixed to the computed local level frame at the beginning of a SAS aperture, l_0. This is the reference frame with respect to which the error equations are expressed.

The starting aperture (and integration) time t_0 is set to 0 without lack of generality. Hence the terms of Eq. (19) are integrated between 0 and the generic time instant t within the SASIT period. From the following definitions where the quantities with the subscript "displ" are displacements with respect to the same quantity computed in t_0 and denoted with a 0 in the subscript:

$$\begin{aligned} \delta\mathbf{p}^c_{eb} &= \delta\mathbf{p}^c_{eb,0} + \delta\mathbf{p}^c_{eb,displ}, \\ \delta\mathbf{v}^c_{eb} &= \delta\mathbf{v}^c_{eb,0} + \delta\mathbf{v}^c_{eb,displ} = \delta\mathbf{v}_0 + \delta\mathbf{v}^c_{eb,displ}, \end{aligned} \tag{B1}$$

it is straightforward to derive:

$$\begin{aligned} \delta\dot{\mathbf{p}}^c_{eb} &= \delta\dot{\mathbf{p}}^c_{eb,displ}, \\ \delta\dot{\mathbf{v}}^c_{eb} &= \delta\dot{\mathbf{v}}^c_{eb,displ}. \end{aligned} \tag{B2}$$

Hence the first equation of (19) becomes by integration:

$$\delta\mathbf{p}^c_{eb,displ} = \int_0^t \delta\mathbf{v}^c_{eb,displ} d\tau + \delta\mathbf{v}_0 t. \tag{B3}$$

By integration of the second and third equations of (19) and using Eq. (3) decomposed in c and Eq. (18), we have:

$$\begin{aligned} &\Delta\psi^c_{cb} = (-\omega^c_{ie} \wedge \psi_0)\, t - \omega^c_{ie} \wedge \textstyle\int_0^t \Delta\psi^c_{cb} d\tau - \int_0^t C^c_b \delta\omega^b_{ib} d\tau, \\ &\delta\mathbf{v}^c_{eb} = -\psi_0 \wedge \textstyle\int_0^t \mathbf{a}^c_{ib} d\tau + (\psi_0 \wedge \mathbf{g}^c_{ib})\, t + \delta\mathbf{g'}_0 t + \int_0^t (\Delta\psi^c_{cb} \wedge \mathbf{g}^c_{ib})\, d\tau + \int_0^t C^c_b \delta\mathbf{f}^b_{ib} d\tau. \end{aligned} \tag{B4}$$

In the first equation of (B4) the second term on the right side can be considered negligible over a SASIT because if the vehicle is assumed to follow a straight line path under constant speed conditions then the average (and the integral) of vehicle attitude misalignment between the instants t_0 and t can be considered as tending to zero. This equation correspond to the second equation of (20).

If the first equation of (B4) is substituted in the second one and the expression:

$$\int_0^t \mathbf{a}_{ib}^c d\tau = \mathbf{v}_{ib}^c - \mathbf{v}_{ib,0}^c \tag{B5}$$

is applied, after a second integration the resulting expression for the position displacement error is:

$$\begin{aligned}\delta\mathbf{p}_{eb,displ}^c = \; & \delta\mathbf{v}_0 t + (\psi_0 \wedge \mathbf{v}_0)\, t - \Big(\psi_0 \wedge \mathbf{p}_{eb}^c + (\psi_0 \wedge \mathbf{g}_{ib}^c)\, \tfrac{t^2}{2} + \mathbf{g}_{ib}^c \wedge (\omega_{ie}^c \wedge \psi_0)\, \tfrac{t^3}{6} + \\ & \mathbf{g}_{ib}^c \wedge \int\int\int C_b^c \delta\omega_{ib}^b d\tau d\tau' d\tau'' + \delta\mathbf{g}'_0 \tfrac{t^2}{2} + \int\int C_b^c \delta\mathbf{f}_{ib}^b d\tau.\end{aligned} \tag{B6}$$

In the following, for the sake of notation simplicity, with $\delta\mathbf{p}_{eb}^c$ it is intended the corresponding displacement error, omitting the subscript "displ". Hence, assumed the Earth mass attraction as exactly known ($\mathbf{g}_{ib}^c = \mathbf{g}_{ib}^{l_0}$), taking into account the definitions in Eq. (21) and after grouping of some terms according to the time polynomial order, Eq. (20) is obtained from Eq. (B6).

Annex C

The navigational simulator/estimator NavLab (FFI-Kjeller)

The navigation simulator/estimator NavLab was developed and made available to SACLANTCEN by NDRE (Norwegian Defence Research Establishment) [4]. It consists of two main parts, a simulator synthesizing measurements from a selected set of navigation sensors by starting from a test configuration defined by the user, and an estimator fusing either real or simulated sensor data and providing the navigation solution by means of a strapdown navigator and an EKF(Extended Kalman Filter)-based [6] integration architecture.

The block diagram of the system is shown in Fig. 23. The set of sensors, the measurement of which can be simulated and integrated, can be reduced or extended.

The sensor simulator consists of:

- a trajectory simulator which provides the true values of the vehicle position, orientation and velocity as the time varies, given the initial position, velocity and orientation of the vehicle and changes in velocity and orientation along the simulated mission;
- a sensor simulator which provides a measurement data set per sensor (i.e., combination of true value and sensor error contributions) as the time varies, given the sensor specifications in terms of error parameters.

At present, the sensor simulator includes the following main error components: white noise, bias repeatability, linear scale factor error.The error stochastic model parameters (e.g., magnitude, time constants, etc.) describing the different error types are user selectable and can be easily deduced from navigation commercial product data sheets. The data sampling rate is also user-selectable.

The strapdown navigator solves the navigation equations presented in Section 2 (see Eq (7), and related Eqs (8), (11), (12) and (15)), which means that, from the IMU raw data (ω_{ib}^b and $\mathbf{f}_{ib}^b$) as provided by real sensors or by the simulator, it provides the navigation solution in terms of body position, attitude and velocity with respect to the Earth. The solution is updated every time a new IMU measurement is available. Errors between the true value and the computed solution of each dynamic variable are evaluable at the navigator output.

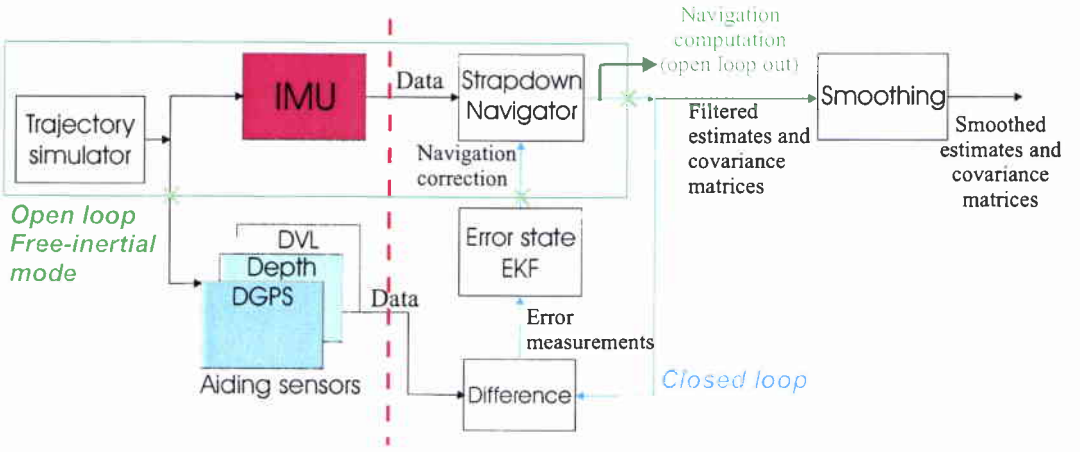

Figure 23 *Block diagram of NavLab architecture. The dashed red line separates the simulator from the estimator. The closed loop is identified by the blue-line path. The green box outlines the blocks used in the present work (open loop - free-inertial mode).*

The EKF-based integrator performs IMU initial alignment and navigation estimation based on multi-sensor data fusion. It works on an error state vector and its outputs are backpropagated to the navigator in order to reset the navigator computation at every EKF step in a closed loop mode (which is outlined in blue in Fig. 23). The estimator includes also an off-line optimal smoothing process on the estimated position.

A user-friendly man-machine interface allows the user to select and plot all the dynamic variables of interest as provided by the simulator, the navigator and the estimator (i.e., variable true values, sensor measurements, navigator solutions and filtered estimates respectively). The expected residual error after filtering is provided in terms of covariance matrices.

NavLab use is limited here to the trajectory simulation on the basis of the selected test configuration, the IMU sensor measurements on the basis of the sensor specifications, and the navigation solution with related error computation (see the green box in Fig. 23). Hence the system is used in free-inertial mode (open loop). Further the accuracy evaluation is performed only on short-time straight-line segments of the simulated trajectory where SAS processing can be applied.

Report no. changed (Mar 2006): SM-368-UU

Document Data Sheet

Security Classification		Project No.
UNCLASSIFIED		03-G
Document Serial No.	**Date of Issue**	**Total Pages**
SM-368	January 2001	59 pp.

Author(s)

Tesei, A., Pinto, M.

Title

Application of aided inertial navigation system to synthetic aperture sonar micronavigation

Abstract

In order to improve short-term navigational accuracy, critical to successful SAS processing, a high-quality Inertial Navigation System (INS) is investigated, which consists of an inertial measurement unit (IMU) and a strapdown navigator. Although the strapdown INS recently acquired at SACLANTCEN is one of the best available, the accuracy of positioning remains insufficient, in particular for high-frequency SAS. The INS performance was predicted via ψ-angle error analysis of the navigation equations and a navigational simulator/estimator provided by NDRE (Norwegian Defence Research Establishment). The short-term residual errors of position and attitude displacement were analyzed in terms of dominant measurement error components and their sources. Preliminary results show that the attitude error is estimated to be negligible due to the low values of gyro bias and white noise. The position displacement error is dominated by a quadratic drift due to accelerometer bias. Integrating the INS with additional navigation sensors (e.g., Doppler Velocity Log, depth meter, etc.) and SAS motion compensation techniques by means of an appropriate architecture will significantly reduce the most critical error components. The design, development and test of the combined SAS-INS architecture will be the main objective of future work.

Keywords

Inertial Navigation Systems – Short-term error mechanisms - Micronavigation

Issuing Organization

North Atlantic Treaty Organization
SACLANT Undersea Research Centre
Viale San Bartolomeo 400, 19138 La Spezia, Italy

[From N. America: SACLANTCEN (New York) APO AE 09613]

Tel: +39 0187 527 361
Fax:+39 0187 527 700

E-mail: library@saclantc.nato.int

The SACLANT Undersea Research Centre provides the Supreme Allied Commander Atlantic (SACLANT) with scientific and technical assistance under the terms of its NATO charter, which entered into force on 1 February 1963. Without prejudice to this main task - and under the policy direction of SACLANT - the Centre also renders scientific and technical assistance to the individual NATO nations.

SACLANT Undersea Research Centre
Viale San Bartolomeo 400
19138 San Bartolomeo (SP), Italy

tel: +39 0187 527 (1) or extension
fax: +39 0187 527 700

e-mail: library@saclantc.nato.int

NORTH ATLANTIC TREATY ORGANIZATION